ADVANCED MATERIALS
www.advmat.de

Nanomaterial-Enabled Stretchable Conductors: Strategies, Materials and Devices

*Shanshan Yao and Yong Zhu**

Stretchable electronics are attracting intensive attention due to their promising applications in many areas where electronic devices undergo large deformation and/or form intimate contact with curvilinear surfaces. On the other hand, a plethora of nanomaterials with outstanding properties have emerged over the past decades. The understanding of nanoscale phenomena, materials, and devices has progressed to a point where substantial strides in nanomaterial-enabled applications become realistic. This review summarizes recent advances in one such application, nanomaterial-enabled stretchable conductors (one of the most important components for stretchable electronics) and related stretchable devices (e.g., capacitive sensors, supercapacitors and electroactive polymer actuators), over the past five years. Focusing on bottom-up synthesized carbon nanomaterials (e.g., carbon nanotubes and graphene) and metal nanomaterials (e.g., metal nanowires and nanoparticles), this review provides fundamental insights into the strategies for developing nanomaterial-enabled highly conductive and stretchable conductors. Finally, some of the challenges and important directions in the area of nanomaterial-enabled stretchable conductors and devices are discussed.

1. Introduction

Flexible electronics has been used in a wide range of applications, such as flexible transistors, smart sensors, flexible energy harvesting and storage, rollable displays, and artificial skins.[1–8] The key advantages of flexible electronics, compared with the flat, rigid counterpart, include high flexibility, low-cost manufacturing (e.g., ink-jet printing and roll-to-roll processing) and inexpensive substrate materials (e.g., plastics). However, flexible electronics faces challenges for applications where devices undergo large deformation (e.g., bending, twisting and stretching) or intimately integrate with curvilinear surfaces (e.g., human skin), which calls for the emergence of stretchable electronics.[9]

Stretchable electronics is a technology that builds electronic circuits on top of a stretchable substrate or by embedding them in a stretchable matrix.[9–14] The past decade has seen exciting progress in the field of stretchable electronics, mainly through the exploration of inorganic materials in addition to organic materials. A common strategy to render stiff, straight inorganic materials stretchable is to create stretchable structures out of them, such as network, mesh, wavy, or coiled shapes. In general, at the system level three architectures/configurations can be employed to achieve stretchable electronics: i) stretchable active device components, ii) stiff active device islands and stretchable interconnects, and iii) a combination of the two.

Two fabrication approaches have been used to process inorganic materials: top-down and bottom-up. Following the top-down approach, stretchable structures can be created for both active device components and interconnects.[15–18] For example, out-of-plane wavy structures have been patterned and transfer printed onto a prestrained substrate followed by releasing the strain to generate wavy structures.[19] In-plane horseshoe-like structures have been fabricated, then transferred to stretchable substrates.[20,21] The top-down approach offers precise microfabrication with excellent repeatability, and thus enables a highly viable route to high-performance stretchable electronics. A variety of exciting devices have been developed using this approach, including hemispherical eye cameras,[22] epidermal electronics,[23] and conformal biointegrated electronics.[24–26]

As a complementary approach, bottom-up synthesized nanomaterials have been demonstrated as building blocks for stretchable electronics. Nanomaterials notably have superior material properties, large surface areas, and are potentially compatible with scalable fabrication processes (e.g., printing). While individually they are much more stretchable than their bulk counterparts (i.e., larger fracture strain[27–32] their stretchability can be further enhanced by introducing stretchable structures.[33,34] So far, progress in nanomaterials for stretchable electronics has been mostly on stretchable interconnects or conductors (i.e., following the 2nd architecture mentioned above), while stretchable active device components using nanomaterials (e.g., stretchable transistors based on carbon nanotubes (CNTs) or graphene[35,36]) are emerging.

In this review, we provide a summary of recent advances in stretchable conductors using bottom-up synthesized nanomaterials over the past five years or so. Among the many nanomaterials that have been reported, carbon nanomaterials and metallic nanomaterials are particularly promising for stretchable conductors and related devices (e.g., capacitive sensors,

S. Yao, Prof. Y. Zhu
Department of Mechanical and Aerospace Engineering
North Carolina State University
Raleigh, NC 27695–7910, USA
E-mail: yong_zhu@ncsu.edu

DOI: 10.1002/adma.201404446

supercapacitors and electroactive polymer actuators), which will be the focus of this review. This review is organized as follows: In Section 2, we summarize the strategies for developing nanomaterial-enabled highly conductive and stretchable conductors. In Section 3–6, we review the recent progress in stretchable conductors based on CNTs, metallic nanowires (NWs), graphene, and metallic nanoparticles (NPs), respectively. In Section 7, we survey the representative applications of the stretchable conductors. Before closing, challenges and future prospects of nanomaterial-enabled stretchable conductors and devices are discussed.

2. Strategies to Render Nanomaterials Highly Stretchable and Conductive

For application as stretchable conductors, it is critical to render nanomaterials highly stretchable and conductive. For stretchability, a straightforward method is to deposit the nanomaterials on top of or to embed them inside elastomeric materials to form composites. Polydimethylsiloxane (PDMS) is a widely used elastomeric material. In order to enhance the adhesion between nanomaterials and a PDMS substrate, surface treatment by oxygen plasma,[37] ultraviolet (UV) light,[38,39] or chemicals[40] has been used to modify the naturally hydrophobic PDMS surface with hydrophilic functionalities. Beyond forming composites, stretchable structures, such as wavy, coiled, net-shaped, spring-like structures are typically introduced to accommodate large deformations.

2.1. Composites

One method to enhance the stretchability is to disperse nanomaterials into elastomeric materials, taking advantage of the electric performances of the rigid filler materials and the mechanical deformability of the soft matrix. Due to their large aspect ratio, 1D nanomaterials are excellent candidates as the filler materials, often in the form of flexible and conductive scaffolds to construct effective conducting networks.[41] The resistance of the resulting composite is generally sensitive to the strain, due to the dependence of the contacts between nanomaterials on the deformation.[42]

To obtain highly stretchable and conductive composites, a delicate balance should be kept between electrical performances and mechanical deformability. High loading of conductive fillers is required for high conductivity, which, however, increases the stiffness and reduces the stretchability of the composite.[43,44] Besides the quality of the filler nanomaterials (e.g., the aspect ratio and purity), the addition of surfactants and the selection of processing methods play a vital role in the quality of the composite (e.g., filler distribution, homogeneity, filler orientation, and resulting mechanical and electrical performances).[45] Homogeneous dispersion of fillers within the surrounding polymer matrix is crucial.[46] Dispersion techniques (e.g., ultrasonication,[44,45] hot pressing,[41] jet-milling,[47] and shear mixing[45,48,49] or exfoliation agents (e.g., ionic liquids [41,44,47,50,51] have been adopted to ensure the uniformity and density of the composite. Perforation and rubber coating[41,50] have been used to increase the elasticity of the composite. Note here the fillers are randomly distributed in the polymer matrix. For more details, a recent summary on the conductive composite elastomers is provided by Jeong and co-workers[52] Besides as fillers, nanomaterials in the form of thin films can be coated/deposited onto or embedded into the elastomeric materials to achieve stretchability.

Typically such nanomaterial filler/polymer matrix and nanomaterial film/polymer matrix composites are stretchable with reasonable conductivity but the conductivity decreases with the applied strain due to the decreased contact area between the nanomaterials as a result of sliding. Only by further introducing stretchable structures, such as net-shaped or wavy structures,[53–56] as discussed in the following sections, could stretchable conductors with stable conductance be achieved.

2.2. With Prestrain

Since the pioneering work of thermally induced buckling of metal thin films on PDMS substrates,[57] there has been much

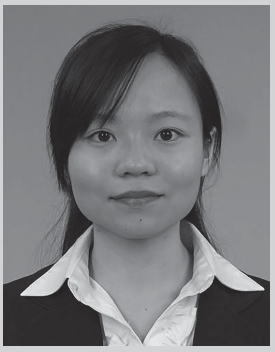

Shanshan Yao received her B.S. in microelectronics and M.S. in microelectronics and solid-state electronics from Xi'an Jiaotong University in 2009 and 2012, respectively. She started Ph.D. studies in mechanical engineering at North Carolina State University from the fall of 2012. Her research interests include growth, nanomechanics, and device applications of nanowires and two-dimensional materials.

Yong Zhu received his B.S. degree in Mechanics and Mechanical Engineering from the University of Science and Technology of China, China, in 1999, and his M.S. and Ph.D. degrees in Mechanical Engineering from Northwestern University in 2001 and 2005, respectively. He was a postdoctoral fellow at the University of Texas at Austin from 2005 to 2007. He is currently an Associate Professor in the Departments of Mechanical and Aerospace Engineering, Materials Science and Engineering and Biomedical Engineering at North Carolina State University. Zhu's research interests include mechanics of nanomaterials, micro/nano-electromechanical systems, and flexible/stretchable electronics.

DOI: 10.1002/adma.201404446

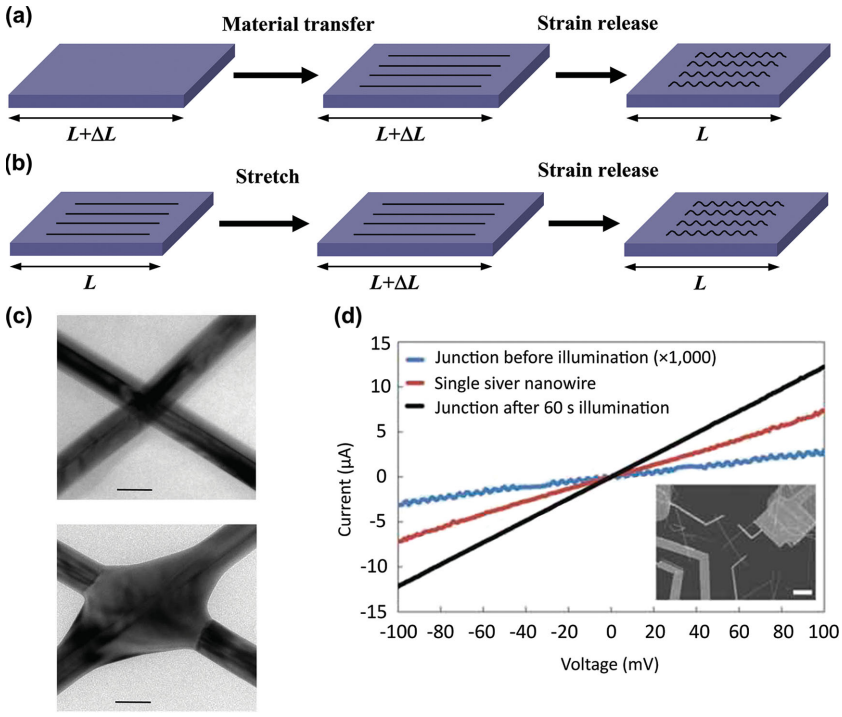

Figure 1. Schematic illustrations of the mechanical buckling processes: a) Prestrain–release–buckling and b) stretching–release–buckling along the longitudinal direction. Plasmonic welding of silver nanowire junctions: c) TEM image of a silver nanowire junction before (top) and after (bottom) illumination. Scale bar is 50 nm. d) The resistance of an individual silver nanowire and a crossed junction before and after 60 s illumination. Scale bar: 2 μm. c,d) Reproduced with permission.[59] Copyright 2012, Nature Publishing Group.

interest in buckling structures for stretchable electronics. Mechanical buckling has been demonstrated to be a promising approach to realize stretchable "wavy" structures on elastomeric substrates. Brittle, inorganic materials could buckle and become stretchable with this approach. The strategy of prestrain–release–buckling is schematically illustrated in **Figure 1**a, which consists of three steps: i) prestraining the elastomeric substrate, ii) transferring or depositing the semiconducting or metallic materials onto the prestrained elastomeric substrate, and iii) releasing the prestrained substrate. The releasing step leads to the spontaneous formation of periodic, wavy structures, which can be bent, stretched, and compressed, similar to an accordion bellows. Upon stretching, the wavy structure accommodates the strain by the increased buckling wavelength and decreased buckling amplitude, rendering much less strain inside the materials themselves. As a result, the electric resistance remains nearly constant during the stretching. The interfacial mechanical properties between the functional materials and the substrate are the key to determine the buckling patterns and related dimensions.[33,54,58]

2.3. Without Prestrain

In the prestrain–release–buckling strategy, a critical step is to prestrain the substrate, which might present a challenge for large-scale manufacturing processes (e.g., the roll-to-roll process). Alternative strategies are being pursued to avoid this prestraining step. One such strategy was recently demonstrated where the interface interaction between the functional materials and the substrate plays an important role.[54] Following this strategy (as shown in Figure 1b), the stretching step is performed after the functional building blocks are transferred/deposited onto the substrate. Upon stretching, the building blocks slide on the substrate (without much strain built in the blocks), but upon releasing the building blocks buckle (instead of sliding back). The resistance typically exhibits a dependence on strain history and achieves a stable value after the release step when a buckled structure is formed.[37,54,60]

Buckling of the building blocks can happen along the longitudinal direction (direction of the tensile strain) or the transverse direction.[61] Due to the Poisson effect, when the substrate is stretched in the longitudinal direction, the building blocks along the transverse direction experience a compressive strain, at a lower level (typically about half for elastomeric substrates). Based on this phenomenon, another strategy to avoid the prestraining step was demonstrated,[61] where the building blocks are transversely oriented. When the substrate is stretched in the longitudinal direction, the transversely oriented building blocks buckle; when the substrate is released, the buckled building blocks recover to their initial flat state. This transverse buckling strategy offers an additional advantage, which is the much reduced strain in the transverse direction compared with that in the axial direction.[61] This strategy particularly applies for 1D nanostructures. The drawback of this strategy is that it only works for uniaxial stretching (not biaxial stretching). All the stretching/releasing steps discussed in this section are after device manufacture.

2.4. Other Stretchable Structures

In addition to the aforementioned strategies, others have been developed to introduce stretchable patterns, such as percolation nanomaterial networks,[62,63] net-shaped structures[37,56,64,65] and spring-like structures.[66] 1D nanomaterials such as CNTs[38,67] and metal NWs[63,68–70] can easily form networks by techniques like dispersing,[60,71] electrospinning,[72] or cross-stacking aligned ribbons.[55] Within a certain level of tensile strain applied, the nanomaterials will rotate and slide against each other to accommodate the strain. Net-shaped structures can accommodate most of the strain by the shape change (alignment of the net along strain direction), and thus maintain the conductive pathways during deformation. The net-shaped structures can be generated by forming fused junctions in the percolation networks (e.g., metal NW percolation network with junctions welded/soldered by graphene oxide[73] and by thermal

annealing[62]), creating reticulate structures by modifying growth condition (e.g., CNT films with continuous 2D reticulate structure[37,64]), and fabricating nanomaterials using templates with network structures (e.g., interconnected networks of graphene grown using a nickel foam template[65] and interconnected networks of carbon nanofibers derived from bacterial cellulose[56]). As another stretchable structure, spring-like structure can be formed by twisting the CNT yarns and the strain is absorbed by straightening the loops.[66]

2.5. Strategies to Enhance Conductivity and Transparency

With the strategies to create stretchable structures, the next question is how to impart high conductivity and even high transparency. The resistance of a nanomaterial network has the contributions from both the nanomaterials themselves and the junctions between them. Generally, the junction resistance is much higher and is the limiting factor for the conductivity of the whole network. In attempt to decrease the junction resistance, techniques such as high-force pressing,[74,75] annealing,[76–78] plasmonic nanowelding[59,79] and soldering by a second materials[73,80,81] have been developed to increase the contact area at junctions or to locally melt the junctions together. A three orders of magnitude decrease in the junction resistance was achieved with light-induced plasmonic nanowelding (Figure 1c–d).[59] The pressing/nanowelding of the junctions work particularly well for metallic NWs, but for CNT and graphene, the low conductivity of the materials themselves represents the main limiting factor of the overall conductivity. Thus doping can be employed to greatly enhance the conductivity of CNTs and graphene.[82–84]

Typically, the higher density of nanomaterials can have better electrical conductivity but at the cost of lower optical transmittance. According to the percolation theory[85,86] for random 2D conducting sticks (or filaments), the critical bonding radius at percolation (R_c) and the stick density (N_s) satisfies Equation 1 and 2:

$$R_c / 2\overline{r_s} = 2.118 \tag{1}$$

$$\overline{r_s} = 1/\sqrt{\pi N_s} \tag{2}$$

which lead to:

$$N_s R_c^2 = 5.71 \tag{3}$$

Clearly, for the case of 1D nanomaterials, the maximum radius for percolation is the length (L) of the conducting NWs or nanotubes and thus the critical density (N_c) to maintain the conductive network for electron transport can be determined by:

$$N_c L^2 = 5.71 \tag{4}$$

The conductivity of the network is given by:

$$\sigma \propto (N - N_c)^t \tag{5}$$

where N is the density of the conducting sticks. For a given density (N) of the NWs/nanotubes, the longer the NWs/nanotubes, the lower the critical density (N_c) is, and thus a higher conductivity can be achieved. The use of longer metallic NWs has been shown to help obtain a better balance between conductivity and transmittance.[62,87] Several figures of merit (FOMs) linking the conductivity and transmittance have been introduced to evaluate the performance of transparent conductors.[88–90]

3. CNT-Based Stretchable Conductors

CNTs can be viewed as molecular-scale tubes of graphitic carbon with outstanding properties, including high mechanical strength, elastic modulus, thermal conductivity, and electrical conductivity.[91,92] They can be synthesized using various methods, such as arc discharge, laser ablation, and chemical vapor deposition (CVD).[93] CNTs can be mass-produced at relatively low cost and therefore have attracted extensive academic and industrial interest.

3.1. CNT/Elastomer Composites

In this section, we focus on stretchable conductors based on CNT composites (e.g., by dispersing CNTs into a polymer matrix). The superior properties of CNTs make them particularly attractive as filler materials to form composites. Due to their remarkable mechanical properties,[94–96] CNT composites are widely used to enhance the Young's modulus, strength, and toughness of different polymer and ceramic systems.[97]

In the past few years, much effort has been devoted to fabricating CNT/polymer composites for stretchable conductors/electrodes, almost all of which are opaque. For instance, single-walled CNT (SWNT) pastes have been prepared by uniformly dispersing chemically stable SWNTs in an elastic fluorinated copolymer matrix.[50] The SWNT pastes were perforated with a net-shaped structure and coated with PDMS to improve their elasticity. The resultant SWNT composite films exhibited initial conductivity of 57 S cm^{-1}, which decreased to 6 S cm^{-1} for a uniaxially applied tensile strain of 134%. The same group then modified the fabrication process by using an ionic liquid and a jet-milling process to ensure the uniform dispersion of longer and finer SWNTs in the fluorinated copolymer matrix.[47] The viscosity of the resulting SWNT rubber composite increased and the extra rubber coating and perforation steps were eliminated, resulting in a process that is compatible with direct printing technologies (**Figure 2**a). The printed elastic conductor can be stretched by 118% with a constant conductivity of 9.7 S cm^{-1} (for 1.4 wt% of SWNTs) or by 29% with a constant conductivity of 102 S cm^{-1} (for 15.8 wt% of SWNTs), as shown in Figure 2b and c.

To further improve the conductivity, Chun et al.[41] reported printable and stretchable composite materials using both micrometer-sized silver flakes and multiwall CNTs (MCNTs) as the fillers, where the MWNTs decorated with silver nanoparticles serve as the flexible scaffolds to bridge the conducting pathways among the silver flakes. The addition of silver was found to greatly improve the conductivity. The hot-rolling

Adv. Mater. 2015,
DOI: 10.1002/adma.201404446

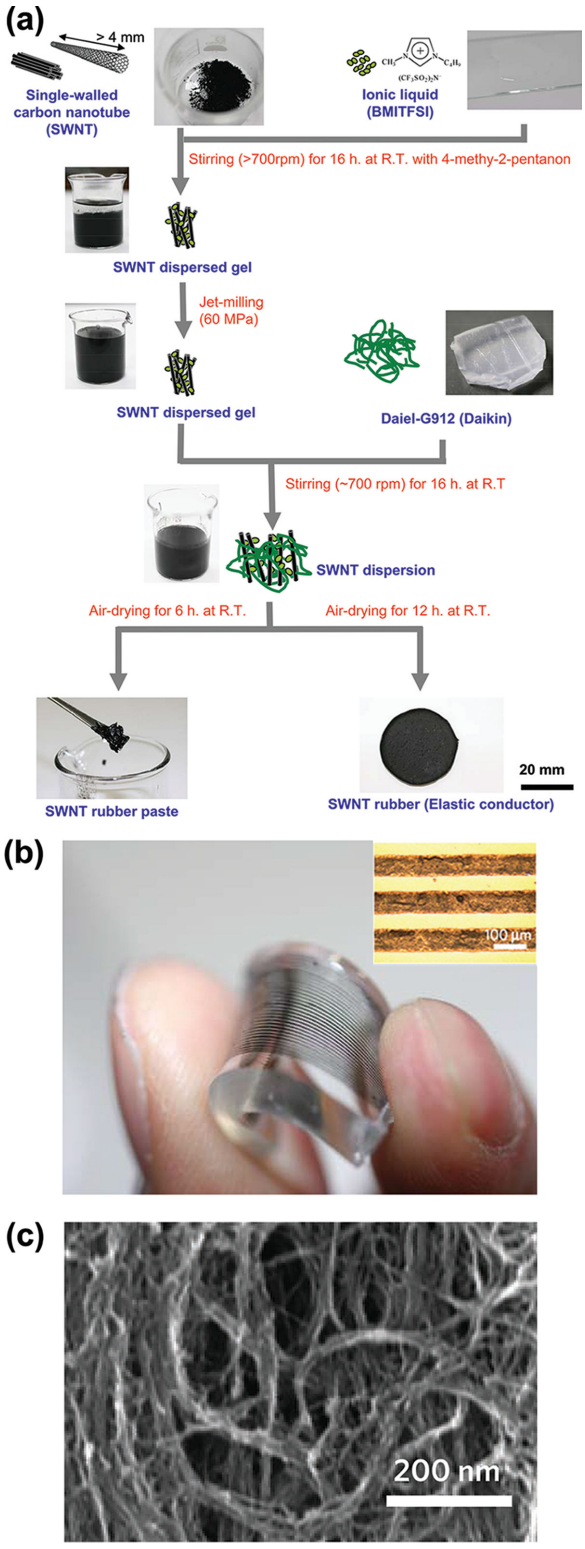

Figure 2. a) Fabrication processes of SWNT film rubber paste and elastic conductor. b) The elastic conductors printed on PDMS sheet using screen printing through shadow masks. The inset shows the microscopy image of the printed elastic conductor. c) SEM image of the elastic conductor. The finer SWNTs were uniformly dispersed and formed well-developed networks in the fluorinated copolymer matrix. a–c) Reproduced with permission.[47] Copyright 2009, Nature Publishing Group.

technique was used to increase the density of the film; the elasticity of the film was improved by perforation and embedding into a nitrile butadiene rubber (NBR) substrate. The maximum conductivity of the hot-rolled and perforated Ag-MWNT/NBR films was found to be 5710 S cm^{-1} at 0% strain and 20 S cm^{-1} at 140% strain.[41] Besides introducing silver to enhance the conductivity of the CNT composite, p-type doping through acid treatment[98,99] offers an alternative way to enable high conductivity at moderately low loading of CNTs, without sacrificing the stretchability of the composites. With a moderately low SWNT content of less than 4 wt%, a very high stretchability was achieved in SWNT–ionic-liquid/silicone-rubber composites sprayed onto an elastic substrate.[44] After nitric acid treatment, the fabricated electrode possessed a high stretchability of 200% and the conductivity was maintained at 18 S cm^{-1} after 20 stretch/release/stretch cycles.

In addition to stretchable and conductive CNT composites fabricated by dispersing CNT powder/ionic liquid in a polymer matrix, progress has been made to develop novel CNT-based stretchable conductors by infiltrating conductive CNTs with soft polymers to form conducting networks. In these materials, the dynamic contacts between the CNTs remain effective during the stretching process. Shin et al.[43] prepared highly elastic and conductive composite sheets by infiltrating MWNT forests with a polyurethane (PU) binder to form 3D accordion-like structures, which showed an extremely high failure strain (over 1400%). The resistance of the film showed little change upon twisting and/or bending. After pretreatment by initial stretching/release cycles, the resistance of the composite sheet remained almost constant for a tensile strain up to 40%. By back-filling highly porous and conducting 3D networks of SWNTs (SWNT aerogels) with PDMS, Kim et al.[100] fabricated stretchable conductors that were mechanically robust against repeated stretching, bending, or twisting deformations. The initial conductivity for the highly transparent SWNT-aerogel–PDMS composite films and the opaque ones were 0.83 S cm^{-1} and 1.08 S cm^{-1}, respectively. The resistance stabilized after five cycles of stretching/release for up to 100% tensile strain.

The performances of stretchable conductors with transmittance lower and higher than 50% are summarized in **Table 1** and **Table 2**, respectively. Commercially available carbon-filled rubber and carbon-particle-based conducting rubber are also included in Table 1 for comparison. For some applications, such as stretchable electrodes for capacitive strain and pressure sensors and electroactive polymer actuators, the conductivity and stable strain range are not critical. However, for other applications, such as stretchable interconnects/electrodes for stretchable displays or integrated electronic circuits, a high conductivity and a large stable strain range are usually required.

3.2. CNT Ribbons/Films

While low-transparency conductors are useful as interconnects and electrodes, making them transparent will broaden the applications of stretchable conductors, such as stretchable displays and solar cells. Doped metal oxides, especially indium tin oxide (ITO), have been the dominant electrode material for optical devices. With the increasing costs due to the scarcity of indium

Table 1. Summary of the performances of stretchable conductors with transmittance <50%. Commercially available carbon-filled rubbers are also included in the table for comparison.

Materials	Strategies	Initial electrical properties	Electrical properties under tensile strain	Applications
SWNT–fluorinated copolymer composite[50]	Composite	σ[a]: 57 S cm^{-1}	σ: Stable at 57 S cm^{-1} within 38% strain	–
SWNT–fluorinated copolymer/PDMS[50]	Composite, Net-shaped structure	σ: 57 S cm^{-1}	σ: Decrease moderately, 6 S cm^{-1} at 134% strain	Stretchable active matrix
SWNT–fluorinated copolymer paste/PDMS[47]	Composite	σ: 102 S cm^{-1} with 15.8 wt% SWNT, 9.7 S cm^{-1} with 1.4 wt% SWNT	σ: Stable at 102 S cm^{-1} within 29% strain, or stable at 9.7 S cm^{-1} within 118% strain	Stretchable active-matrix displays
Ag–MWNT–fluorinated copolymer/NBR[41]	Composite, Net-shaped structure	σ: 5710 S cm^{-1}	σ: Decrease with strain, 20 S cm^{-1} at 140% strain	Stretchable LED interconnects
Nitric acid-doped SWNT-KE441/acrylic elastomer[44]	Composite	σ: ca. 63 S cm^{-1}	σ: Stable at 18 S cm^{-1} within 200% strain	–
MWNT forests–PU[43]	Composite	σ: 0.5–1 S cm^{-1}	R[c]: Almost constant for strain up to 40%	–
MWNT–PDMS composite[45]	Composite	σ: ca. 10^{-5} S cm^{-1}	R: Increase with strain	–
SWNT aerogel–PDMS[100]	Composite	σ: 1.08 S cm^{-1}	R: Stable within 100% strain	–
Au/Pd-coated superaligned MWNT ribbon/PDMS[53]	Prestrain (100%)-releasing-buckling, Composite	R_s[b]: 72 Ω sq^{-1}	R: Stable within 100% strain	Stretchable LED interconnects
Superaligned MWNT ribbon/PDMS[54]	Stretching–release–buckling, Composite	R_s: 211 Ω sq^{-1} (T: 40%)	R: Stable within 100% strain	–
Cross-stacked Superaligned CNT film-PDMS[55]	Cross-Stacked structure, Composite	σ: 63 S cm^{-1}, R_s: 405 Ω sq^{-1}, T[d]: 39% for 4 layers	R: Increase by 15% at 28% strain	–
SWNT/VHB 4905[71]	Composite, Network	R: ca. 300 Ω	R: Superlinearly increase, ca. 10^7 Ω at 700% strain	Dielectric elastomer actuators
Reticulate SWNT/PDMS[101]	Net-shaped structure, Prestrain (100%)-releasing-buckling, Composite	–	R: Stable within 140% strain	Stretchable supercapacitors
SWNT/PDMS[38]	Prestrain (40%) releasing-buckling, Composite	–	R: Stable within 40% strain	Stretchable supercapacitors
SWNT/PDMS[102]	Composite	R_s: ca. 170 and ca. 19 Ω sq^{-1} for 1 and 5 layers	R: Increase by less than 1.2 times within 100% strain	Stretchable LED interconnects
Superaligned CNT/PDMS[103]	Prestrain (100%)-releasing-buckling, Composite	R_s: ca. 650 Ω sq^{-1}	R: Increase by less than 6% within 100% strain	–
CNT rope[66]	Spring-like structure	σ: 440 S cm^{-1}	R: Increase by 2% at 20% strain	–
CNT fiber/PDMS[104]	Prestrain (40%)-releasing-buckling, Composite	–	R: Almost stable within 40% strain	–
Carbon fiber/PDMS[56]	Composite, 3D interconnected network	σ: 0.20–0.41 S cm^{-1}	R: Almost stable within 80% strain	Stretchable LED interconnects
AgNW–PDMS[60]	Composite, Network, Stretching (80%)–release–buckling	σ: ca. 8130 S cm^{-1}	σ: Stable at 5285 S cm^{-1} within 50% strain	Capacitive sensors, Stretchable LED interconnects
AgNW–PDMS[105]	Composite, Network	R: 9.8 Ω	R: Increase with strain up to 100%	Stretchable batteries
AgNW–CNT/Ecoflex[79]	Composite, Network	R_s: 18 Ω sq^{-1}	R: Increase with strain up to 480%	Stretchable LED interconnects
AgNW–CNT/Ecoflex[106]	Prestrain (150%)–release–buckling, Composite, Network	R_s: 24–27 Ω sq^{-1}	R: Increase with strain up to 460%	Stretchable LED interconnects
PUS–AgNW–PDMS[107]	Composite, 2D/3D binary networks	σ: 8.35–19.2 S cm^{-1} depending on the mass content	R: Increase by 160% at 100% strain for the first cycle	Stretchable LED interconnects
3D AgNW–PDMS[108]	Composite, 2D/3D binary networks	σ: 21.5 S cm^{-1} with AgNW density of 25 mg cm^{-3}	R: Increase by 150% at 100% strain, almost stable within 50% strain after the second stretching	Stretchable LED interconnects

Adv. Mater. **2015**,
DOI: 10.1002/adma.201404446

Table 1. Continued

Materials	Strategies	Initial electrical properties	Electrical properties under tensile strain	Applications
CuNW/VHB 4905[109]	Composite, Network	–	Conductive within 200% area strain	Dielectric elastomer actuators
CuNW–PVA–PDMS[110]	Porous structure, Composite	σ: 0.83 and 8.1 S cm^{-1} (annealed) with PVA concentration of 10%	*R*: Almost stable within 60% strain	–
Ag-doped graphene fibers/PDMS[83]	Prestrain (150%)–release–buckling, Composite	σ: 930 S cm^{-1}	Conductive for 150% strain	Stretchable LED interconnects
Graphene/VHB 4905[111]	Composite, Biaxially prestrain(10%, 500%)–release–buckling	*R*: ca. 8000 Ω (*T*: 30%)	*R*: Increase with strain up to 450%	Dielectric elastomer actuators
GF–PDMS[65]	Composite, 3D interconnected network	σ: ca. 10 S cm^{-1}	*R*: Increase by ca. 30% at 50% strain	–
AgNP/SBS fiber mat[112]	Composite	σ: 5400 S cm^{-1}	σ: Decrease with strain, 2200 S cm^{-1} at 100% strain	Stretchable antenna, LED interconnects, strain sensors
AgNP/wavy PDMS[113]	Wavy structure, Composite	–	*R*: Increase by ca. 3 times at 30% strain	–
AgNP/PU[114]	Composite, 3D network	σ: 11 000 S cm^{-1} and 1800 S cm^{-1} for 5 × LBL and 5 × VAF composites	σ: Decrease with strain, and 2400 S cm^{-1} and 94 S cm^{-1} at 110% strain for 5 × LBL and 5 × VAF composites	–
Au nanosheet/SBS mat[115]	Network	σ: ca. 33 333 S cm^{-1}	Almost stable within 90% strain	Stretchable transistors
Carbon-filled rubber (Stockwell Elastomerics, Inc.)[43]	–	σ: 0.02–0.2 S cm^{-1}	Strain at break: 100–275%	–
Carbon particle-based conducting rubber (Kinugawa Rubber Industrial)[50]	–	σ: ca. 0.1 S cm^{-1}	σ: Almost stable within 160% strain	–

[a] σ: Conductivity; [b] R_s: Sheet resistance; [c] *R*: Resistance, [d] *T*: Transmittance.

and other limitations, including poor flexibility, dramatically deteriorated conductivity under strain, and limited transparency in the near infrared region,[126] new stretchable and transparent electrodes are in demand to replace ITO.[127,128] CNTs, metallic NWs, and graphene are all promising candidates.

To date, two main methods have been employed to fabricate CNT-ribbon/film-based conductors: i) CNT ribbons consisting of aligned CNTs directly drawn from vertically grown CNT forests, and ii) deposition or embedding of randomly distributed CNTs onto or inside stretchable substrates such as PDMS. These methods are employed along with other strategies discussed in Section 2 to fabricate highly conductive, transparent, and stretchable conductors based on CNT ribbons/films, which have shown promising potential for stretchable devices, including stretchable displays[47] loudspeakers,[129] pressure and strain sensors,[39,130] and stretchable supercapacitors.[38,101]

CNT ribbons are sheets of continuous and unidirectional CNTs, in which the CNTs are uniform and aligned nearly parallel to the drawing direction.[131] The key to producing CNT ribbons is to fabricate high-quality, superaligned, vertically grown CNT forests.[132] To distinguish from an ordinary, vertically aligned CNT forest, superaligned CNT forests have much better alignment and stronger van der Waals interactions, and can be drawn into continuous films or yarns,[133–135] which originates from their very clean surface, narrower diameter distribution, and higher nucleation density.[131,136] Superaligned CNT forests are typically grown by low-pressure CVD and **Figure 3**a shows a typical SEM image of a superaligned, vertically grown CNT forest. The drawing process from superaligned CNT arrays to films and yarns is quite simple, where CNT bundles are joined end-to-end and aligned along the drawing direction, as schematically shown in Figure 3b. A continuous ribbon can be obtained simply by using tweezers to pick off or blades to scratch off CNT bundles from the superaligned CNT array.[131] The as-drawn CNT ribbons are unidirectionally aligned, ultrathin (tens of nanometers), extremely lightweight, transparent, and conductive, and they can be fabricated in a large size by the roll-to-roll process.[129,131,137] Figure 3c shows an optical image of a transparent conducting film drawn from a superaligned CNT forest/array. When preparing CNT ribbons and yarns, volatile solvents (e.g., ethanol or acetone) are commonly used to shrink the yarns/ribbons[53,55,132,138,139] or increase the density of the cross-stacked superaligned CNT films,[55] mainly for two reasons: i) better interaction among the CNTs and thus better mechanical strength, and ii) decreased surface roughness leading to reduced light scattering but higher transmittance. The transmittance of a CNT film can be improved by reducing the height of the superaligned CNT arrays through controlling the growth conditions[136] and laser or oxygen-plasma trimming of the superaligned CNT arrays and as-drawn CNT ribbons.[137] The conductivity can be enhanced by metal deposition[53,137] and chemical doping.[37,39,82] Ultrathin CNT films have been

Table 2. Summary of the performances of transparent stretchable conductors with transmittance >50%.

Materials	Stretchable Strategies	Initial electrical properties,[a] T[b]	Electrical properties[c] under tensile strain	Applications
Superaligned MWNT ribbon–PDMS[116]	Stretching–release–buckling, Composite	60%	Stable at 3.5 kΩ within 100% strain	–
Superaligned MWNT ribbon/PDMS[116]	Prestrain (50%), Composite	–	Stable within 50% strain	–
CNT/PtBA[67]	Composite	Composite: 500, 87%	Resistance increase with strain up to 50%	Polymer light-emitting electrochemical cells (PLECs)
Doped SWNT film/PDMS[39]	Stretching–release–buckling, Composite	SWNTs: 328 Ω sq^{-1}, 79%; 1100 S cm^{-1}, 68% for a 100 nm film	σ[d]: Stable at 2200 S cm^{-1} within 150% strain	Strain and pressure sensors
Reticulate SWNT film–PDMS[37]	Net-shaped structure, Composite	53, 62%; 20, 52%; 7, 16%	Stable within ca. 40% strain	Stretchable LED interconnects
Acid-treated SWNT–PU nanoweb/VHB[117]	Stretching–release–buckling, Network, Composite	SWNT–PU: 424, 63%	Almost stable within 100% strain	–
SWNT aerogel–PDMS[100]	Composite	Composite: 0.83 S cm^{-1}, ca. 93%	Stable within 100%	–
Ultralong AgNW/Ecoflex[62,76]	Prestrain (300%), Composite, Network	AgNWs on glass: 9, 89%; 69, 95%	Slightly increase within 460% strain	Stretchable LED interconnects
AgNW–polyacrylate with 5% AA[69]	Composite, Network	AgNWs: 50.1, 92.4%; 7.4, 81.7% Composite: 50.8, 90.2%; 7.5, 79.6%	Increase with strain, 2.3 times at 50% strain.	–
AgNW–PtBA with 5% AA[68]	Composite, Network	Composite: 88.6, 80%; 10, 45%	Increase with strain, within 10^3 Ω sq^{-1} (R_s) at 140% strain	Bistable large strain actuation
AgNW/PU[118]	Composite, Network	Composite: 44.7, 82.7%; 8, 74.6%	Increase with strain, highly conductive at 60%	Capacitive sensors
AgNW/dopamine-modified PDMS[40]	Composite, Network	Composite: 35, 80%	Almost stable within 15% strain	Flexible LED interconnects
AgNW/PDMS[119]	Prestrain (10%) in both axis, Composite	AgNWs: 14, ca. 85%	Biaxially stable within 5% strain	Stretchable LED interconnects
AgNW–PDMS–Zonyl[120]	Composite, Network	Composite: 4.5, 80%	Increase with strain up to 100%	Stretchable LED interconnects, stretchable photodetectors
PEDOT:PSS–soldered AgNW/PEN[80]	Composite, Network	AgNWs: 600, 90%; 25, 85%	Increase with strain up to 20%	Flexible Touch-Panels
GO-soldered AgNW–PUA[73[	Net-shaped/fishnet structure	AgNWs: 26, 92.1%; 12, 86% Composite: 26, 86.3%; 12, 79.2%	Increase with strain, 10.6 times increase at 80% strain	Stretchable polymer LEDs
AgNP/PDMS[121]	Zigzag structure, Composite	ca. 10^4 S cm^{-1} (σ) for uniaxial stretchable conductor; ca. 70% (T) for biaxially stretchable conductor	Highly conductive under ca. 50% uniaxial stain; for double-transferred sample, conductive under 40% biaxial strain	Stretchable LED interconnects
CuNW–poly(acrylate)[122]	Composite, Network	Composite: 220, 91.5%; 5, 70.5%	Increase with strain for strain up to 15%	–
CuNW–PU[70]	Composite, Network	CuNWs: 52, 86.7%; 8, 70.7% Composite: ca. 56, 84.5%; ca. 8, 68.7%	Increase with strain, below 100 Ω sq^{-1} for strain up to 60%	–
CuNW/Ecoflex[63]	Composite, Network	CuNWs: 37, ca. 80%	Increase slowly with strain up to 250%	Touch panels
CuNF/PDMS[72]	Composite, Network	CuNWs: 200, ca. 96%; 50, ca. 90%; 12, 80% Composite: 9.2, 50%	Increase by 5% at 10% strain	–

Adv. Mater. **2015**,
DOI: 10.1002/adma.201404446

Table 2. Continued

Materials	Stretchable Strategies	Initial electrical properties,[a] T[b]	Electrical properties[c] under tensile strain	Applications
Graphene/PDMS[123]	Composite, Isotropically prestrain (12%)	Graphene on quartz plate: ca. 280, ca. 80%	Stable biaxially within ca. 11%, increase by one order of magnitude at ca. 25% strain	–
PVA/Wavy Graphene/PDMS[124]	Wavy structure, Composite	Graphene: 600–1250, PDMS supported Graphene: 50–60% (T)	Increase with strain, ca. 2 times at 40% strain	Stretchable Supercapacitors
Graphene–AgNW/PDMS[125]	Network, Composite	Graphene–AgNWs: 33, 94%	Almost stable within 100% strain	Oxide semiconductor transistors, Stretchable ILED interconnects

[a]Sheet resistance (unit: Ω sq^{-1} unless otherwise indicated); [b]T: Transmittance; [c]Resistance unless otherwise indicated; [d]σ: Conductivity.

employed in a myriad of applications, such as polarizers and polarized light sources,[133,134] incandescent displays,[140] surface-enhanced Raman scattering (SERS) substrates,[141] transmission electron microscopy (TEM) grids,[142] and CNT touch screens.[137]

Due to their unique properties, promising stretchable conductors have been fabricated either by creating wavy structures out of otherwise-flat CNT ribbons or by using cross-stacked CNT ribbons. Zhang et al.[116] fabricated transparent stretchable conductors by embedding continuous CNT ribbons into PDMS. The CNT–PDMS film showed a transparency of ca. 60% at wavelengths ranging from 400 to 800 nm, and excellent flexibility and robustness. Under the first stretching, the CNTs slid against each other, leading to improved alignment along the tensile direction and weakened CNT connections, and thus to an increase in resistance. Upon release, wavy structures were generated accompanied by better connections between the CNTs. As a result, only a small fraction of the resistance was recovered. After the wavy structure was formed, a stable resistance (35.5 kΩ) was achieved for strains up to 100% after six stretching/release cycles.

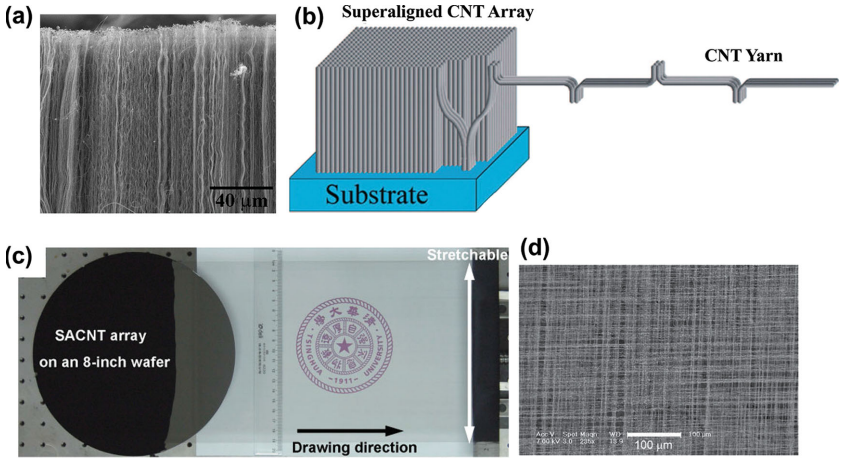

Figure 3. a) Side-view SEM image of the vertically grown CNT forest. Reproduced with permission.[53] Copyright 2012, John Wiley and Sons. b) Schematic illustration of drawing yarns or films from superaligned CNT arrays. Reproduced with permission.[131] Copyright 2011, John Wiley and Sons. c) A transparent conducting film drawn out of superaligned CNT arrays on an 8-inch silicon wafer. Reproduced with permission.[137] Copyright 2010, John Wiley and Sons. d) SEM image of a 2-layer cross-stacked superaligned CNT film. Reproduced with permission.[55] Copyright 2011, John Wiley and Sons.

With a similar stretching–release–buckling strategy, our group fabricated transparent stretchable conductors based on CNT ribbons after the device manufacture.[54] Here, the CNT ribbons were transfer printed onto the top of a PDMS substrate to investigate the detailed microstructural changes of the aligned CNTs under strain, which was not possible in previous work[116] where the CNT ribbons were embedded in PDMS. It was observed that during stretching, the CNTs slid on the substrate and between themselves, which caused the increase in resistance; during release (compression), the CNTs formed periodic wavy structures in the lateral direction (in-plane), as shown in **Figure 4**a. Upon formation of the wavy structures, the resistance of the CNT ribbon remained constant during the following stretching and release cycles, as shown in Figure 4b. A continuum-mechanics analysis based on the shear-lag theory was performed to correlate the observed sliding behavior with the interfacial mechanical properties between the CNTs and the PDMS. A stable resistance can be achieved in CNT-ribbon/PDMS conductors in a wide strain range (>100%).

Using the prestrain–release–buckling strategy, CNT ribbons were transfer printed on top of a prestrained PDMS substrate to fabricate transparent stretchable conductors.[53] Release of the prestrain caused out-of-plane buckling of the CNT ribbons (Figure 4c). The wavy CNT ribbons were able to accommodate large stretching up to the prestrain level (100%) with an increase in resistance of only about 4.1%, as shown in Figure 4d. Note the resistance is normalized by its initial value at the zero strain. The small resistance change is due to the existence of flat regions, where the CNTs slide under the applied strain. At a strain higher than the prestrain, the CNT ribbons showed a strain dependence of the resistance because of the sliding between the CNTs, similar to the stretching–release–buckling scenario. By coating the CNTs with a thin layer of sputtered Au/Pd, a fairly high electrical conductance was obtained. Applying the same prestrain–release–buckling strategy, the vertically aligned CNTs were patterned and transfer printed with the assistance of a PDMS stamp, infiltrated with PDMS, and then bonded to the prestrained PDMS substrate, and a

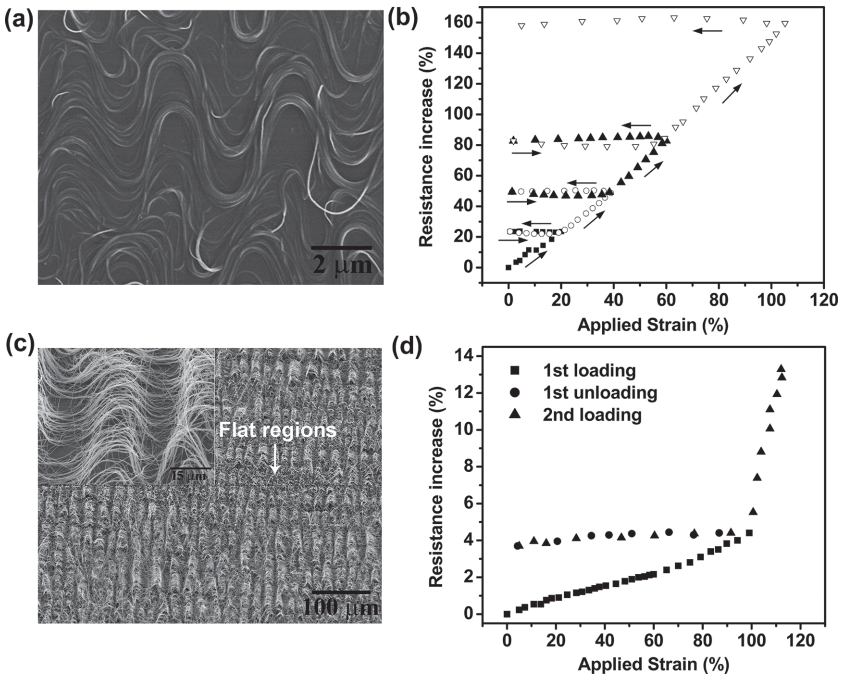

Figure 4. CNT ribbon/PDMS stretchable conductor by the stretching–release–buckling strategy: a) An SEM image showing the lateral buckling of CNTs induced by stretching–release–buckling. b) Resistance change of a CNT film on top of PDMS as a function of applied strain. a,b) Reproduced with permission.[54] Copyright 2012, John Wiley and Sons. CNT ribbon/PDMS stretchable conductor by the prestrain–release–buckling strategy: c) SEM image of a buckled CNT ribbon induced by releasing the prestrain of PDMS. Inset shows the high magnification image. The images were taken by tilting the sample at an angle of 20°. d) Resistance of a CNT ribbon/PDMS film as a function of tensile strain. c,d) Reproduced with permission.[53] Copyright 2012, John Wiley and Sons.

resistance increase of less than 6% was observed for stretching up to the prestrain level (100%).[103]

In addition to a single layer of CNT ribbons, cross-stacked CNT ribbons,[141–144] were used to create a cross-shaped conducting net (Figure 3d). A stretchable conductor made of even layers of cross-stacked, superaligned CNTs embedded into PDMS showed a small resistance change within a strain of 28%.[55] The advantage of cross-stacked CNT-ribbon/PDMS over single layers of CNTs is the isotropic electrical conductivity, making it potentially a biaxial transparent and stretchable conductor.[55]

In the second method, randomly distributed CNT films, with or without reticulate structures, deposited on top of or embedded inside elastomeric substrates have been demonstrated as transparent and stretchable conductors. The most commonly used elastomeric substrate is PDMS, while other materials have been used.[67,71] CNTs can be formed into thin films by simple solution dispersion using methods like spray-coating[39,71] and Meyer-rod-coating.[67] Alternatively, CNTs can be embedded in elastomeric substrates by over-coating the elastomeric material on a CNT film, followed by polymerization of the elastomer.

Randomly distributed SWNTs sprayed onto a VHB 4905 substrate (from 3M) maintained a high conductivity under very high strains up to 700%, but the resistance increased with strain.[71] Lipomi et al.[39] deposited transparent CNT films on a PDMS substrate; upon stretching and release of the strain, a spring-like structure made of CNTs (**Figure 5**a) was generated. The successful application of the stretching–release–buckling strategy enabled the CNT/PDMS composite to be stretchable for strains up to 150% while maintaining a high conductivity (2200 S cm^{-1}) in the stretched state. When stretching and releasing the substrate in both axes, the films exhibited buckling structures and stretchability in both directions (Figure 5b). In other work, 2D SWNT macrofilms were rendered stretchable by creating periodically sinusoidal patterns through the prestrain–release–buckling method (Figure 5c).[38] The SWNT films were able to maintain a stable conductance within the strain range up to the prestrain level (40%). Very recently, an inkjet-printed SWNT-based stretchable conductor was reported.[102] Sheet resistances of ca. 170 and ca. 19 Ω sq^{-1} were realized for 1- and 5-layer printed films after nitric acid treatment. A resistance increase of

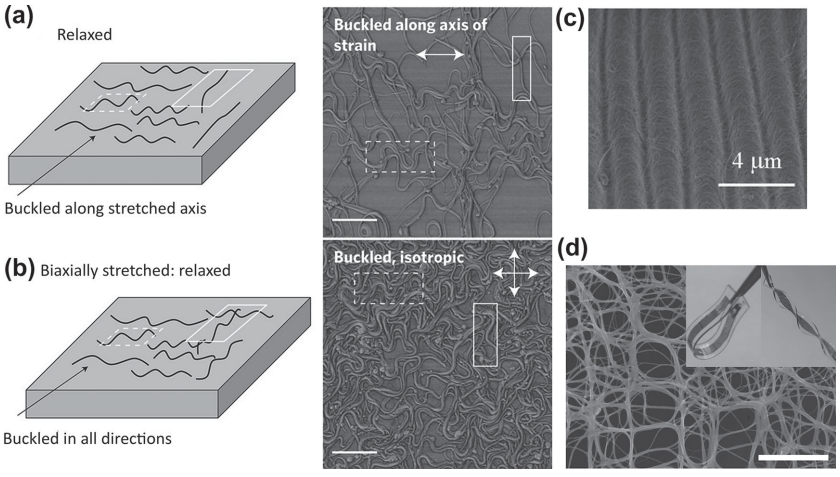

Figure 5. Schematics (left) and corresponding AFM phase images (right) of CNT films on PDMS after stretching and releasing the PDMS along one axis (a) and along two axes (b). Scale bars: 600 nm. The dashed and solid white boxes indicate the CNT bundles buckled along the horizontal and vertical axes, respectively. a,b) Reproduced with permission.[39] Copyright 2011, Nature Publishing Group. c) SEM image of a buckled SWNT macrofilm on PDMS, where the buckling wavelength is 2 μm. Reproduced with permission.[38] Copyright 2009, John Wiley and Sons. d) SEM image of the as-grown single walled carbon nanotube films with hierarchical reticulate structures. The inset shows photographs of SWNT/PDMS stretchable conductor under bending and twisting. Scale bar: 500 nm. Reproduced with permission.[37] Copyright 2012, John Wiley and Sons.

Adv. Mater. **2015**,
DOI: 10.1002/adma.201404446

less than 20% was observed after the 5-layer film was subjected to 100% tensile strain for 1000 cycles.

SWNT films with a hierarchical reticulate structure (Figure 5d) synthesized via floating-catalyst CVD possess a high conductivity (2000 S cm^{-1}) and a high strength (350 MPa) owing to the unique 2D reticulate structure and the long inter-bundle connections.[64] By embedding this unique structure into PDMS, Cai et al.[37] created highly transparent and stretchable conductors. The transmittance ranged from 62% to 16% at a wavelength of 550 nm with sheet resistance ranging from 53 to 7 Ω sq^{-1}. After the first several cycles of stretching/release, it was observed that the film became reversibly stretchable without much resistance change under a certain strain range (ca. 40%). The fracture strain was found to be 60% with a resistance increase of 125%. Taking advantage of the initial stretchability of the continuous 2D reticulate SWNT structure and the buckling surfaces that were rendered by prestraining and releasing a PDMS substrate, a stable resistance was achieved in the strain range of 140%.[101] For strain within 100%, the CNT–PDMS electrodes accommodated the strain mainly by the buckled patterns, while beyond that, the strain was largely absorbed by the deformation of the 2D reticulate SWNT bundles along the strain direction.

3.3. CNT Fibers and Yarns

Another interesting CNT assembly that can be used for stretchable conductors is CNT fibers or yarns, which have the potential to retain the excellent mechanical and electrical properties of the individual CNTs.[104] The CNT fibers can be produced by continuously dry- or wet-spinning of bunches of CNTs from vertically superaligned CNT arrays,[133,135,145,146] CNT solutions,[147] melts with dispersed CNTs,[148] or gas-phase aerogels of CNTs.[149,150] The fabricated CNT yarns typically show a very high strength-to-weight ratio[150] and a high conductivity.[146] Applications such as strain sensors,[151] tough composite fibers,[152,153] high-strength and highly conductive composites,[138] and torsional artificial muscles[154] have been demonstrated. The main limitation of CNT yarns for stretchable electronics is the limited stretchability, which is due to the irreversible sliding between the CNTs during stretching.[42,66,155] The strain-to-failure values were generally less than 10%,[135,150] for either as-fabricated yarns or yarns after alcohol and thermal treatments.[132] Besides the early fracture at small strains, the sliding and irreversible deformation also deteriorate the conductivity of the yarns, showing as a rapid increase in resistance under strain.

To impart stretchability to the CNT yarns, two approaches have been developed: over-twisting the CNT yarns to form a spring-like structure[66] and prestrain–release–buckling.[104] Representative structures following the two approaches are shown in **Figure 6**. In the first approach, the CNT yarns were slightly over-twisted to generate a spring-like rope with self-assembled loops (Figure 6a–c). Under stretching, the rope can accommodate the strain by separating and straightening the loops, somewhat similar to the wavy or net-shaped structures. The reported stretchability is as high as 285%, 20 times higher than that of the original, straight CNT yarns.[66] Besides the super-stretchability, the spring-like rope exhibits good strength, stable spring constants (within 20% tensile strain), and conductivity: The initial conductivity was 440 S cm^{-1}, which remained stable within a moderate strain of 20% for 1000 loading cycles.

Using the second approach, Zu et al.[104] fabricated CNT-fiber-based stretchable conductors by releasing a prestrained PDMS substrate with the transferred CNT fibers on top. To enhance the interfacial bonding between the CNT fibers and the PDMS and facilitate the buckling of the CNT fibers, a thin layer of liquid PDMS was coated on top of the CNT fibers. While also using the prestrain–release–buckling method, the generated buckling shape is quite different from those for individual CNTs,[156] CNT films,[38] well aligned CNT ribbons,[53,54] silicon NWs,[33] and silicon nanoribbons.[157] Instead of sinusoidal or coil shapes, the CNT fibers kink laterally, as shown in Figure 6d. During the stretching/release cycle, the kinked pattern accommodates the strain by straightening and kinking back without apparent permanent fracture. An almost stable resistance was observed for strain levels up to the prestrain level (40%).

In addition to the yarns and fibers made of CNTs, polymer fibers coated with nanomaterials are emerging as conductors.[117,158,159] An acid-treated SWNT/PU nanoweb was reported as a transparent stretchable conductor, where electrospun PU fibers were used as the stretchable template/scaffold to guide the deposition of the CNTs without agglomeration. A conducting network with a small amount of CNTs was formed, with a sheet resistance of 424 Ω sq^{-1} at 63% transmittance. By generating noodle-like structures in PU fibers by the stretching–release–buckling strategy (Figure 6e), the CNT/PU nanowebs exhibited almost constant conductivity under strains up to 100% after several cycles of stretching and release.[117]

4. Metal-Nanowire-Based Stretchable Conductors

Despite the exciting progress of CNT-based stretchable conductors, their conductance is still quite low (Table 1 and 2). Conductors with relatively low conductance are acceptable in voltage-driven devices (e.g., capacitive touch screens, electrowetting displays, and liquid-crystal displays), but not for current-driven devices like organic light-emitting diodes (OLEDs) and solar cells.[126] Metal materials including thin metal films,[160,161] metal grids,[162,163] and metallic NWs have received much attention due to their high conductivity and ductility (i.e., large failure strain). While thin metal films and metal grids are promising as transparent electrodes,[90] their rigid nature limits their application in stretchable electronics. On the other hand, networks of metallic NWs are rather attractive as stretchable conductors.

4.1. Silver Nanowires

Among all the metal materials, Ag has the highest electrical conductivity,[164] by virtue of which silver NWs (AgNWs) are the most extensively studied metal nanostructures as conductors. AgNWs can be grown by a variety of methods,[165] including the hydrothermal method, the polyol synthesis process, the

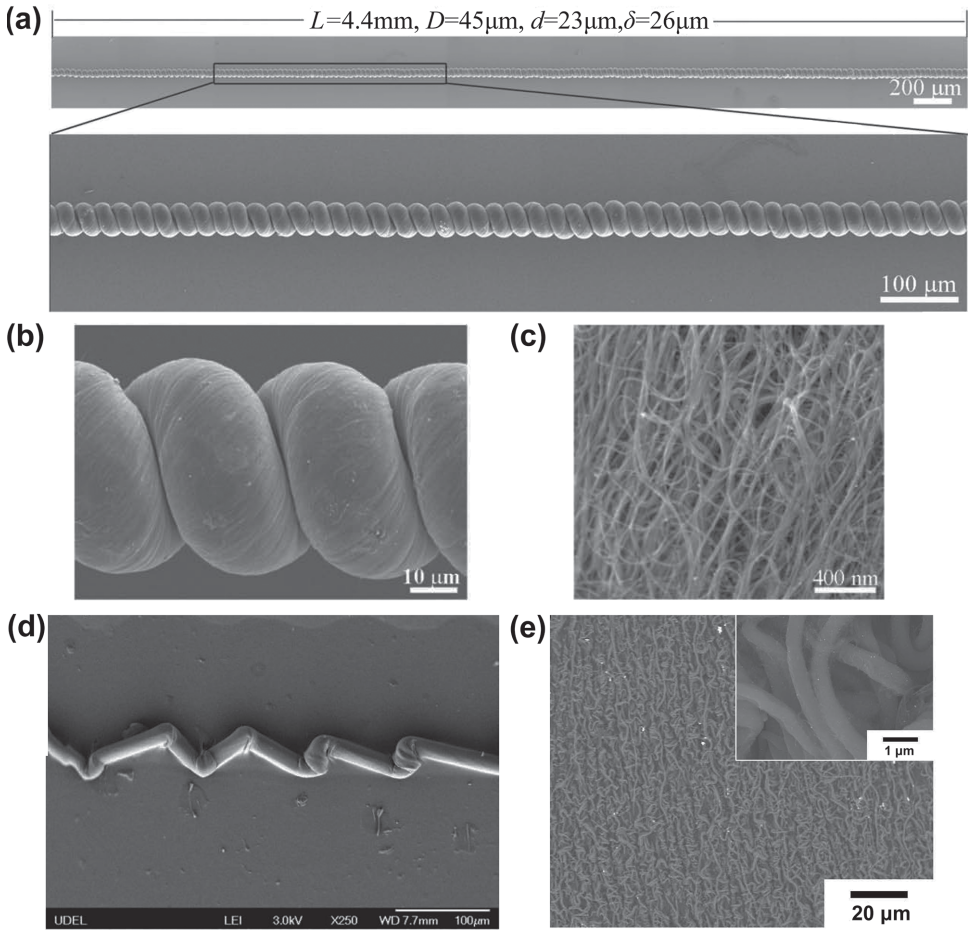

Figure 6. SEM images of yarn-derived spring-like CNT rope: a) SEM image showing highly uniform, perfectly arranged loops. b) High magnification image of the loops. c) SEM image of the loop surface showing single-walled nanotube bundles. a–c) Reproduced with permission.[66] Copyright 2012, John Wiley and Sons. d) SEM image of the kinked CNT fiber showing the in-plane kinked patterns enabled by prestrain-then-release the PDMS substrate. Reproduced with permission.[104] Copyright 2013, John Wiley and Sons. e) SEM images of SWNT/PU nanoweb with noodle-like structure induced by the stretching–release–buckling strategy. The inset shows the magnified image. Reproduced with permission.[117] Copyright 2012, Royal Society of Chemistry.

microwave-assisted process, the electrochemical technique, the UV irradiation technique, and the template technique, among which the polyol synthesis process[166–169] is relatively simple with low cost and a high yield, and is thus widely used. In the polyol possess, metallic precursors (e.g., silver nitrates) are reduced by a polyol (e.g., ethylene glycol) with the presence of poly(vinylpyrrolidone) (PVP). AgNWs are typically grown with diameters of 30–200 nm and lengths of 1–20 μm.[127] Recently, Lee and co-workers developed a successive multistep growth method for very long AgNWs, where $AgNO_3$ was reduced repeatedly in ethylene glycol in the presence of PVP.[62,76] **Figure 7**a–c show the very long AgNW ink, an SEM image, and the transparent electrode made of such AgNWs, respectively. The average length and diameter after seven reduction steps of $AgNO_3$ were reported to be 96.1 μm and 160 nm, respectively.

Besides excellent electrical conductivity, AgNW networks show a high transmittance for a wide range of wavelengths. In contrast, the transmittance of ITO electrodes deteriorates in the near-infrared.[126] AgNWs also exhibit an interesting surface plasmon resonance property arising from collective oscillations of the conduction-band electrons upon interaction with the incident electromagnetic field.[170,171] Taking advantage of the surface plasmonic property, AgNWs have been used in a wealth of applications, including ultrasensitive biosensing[172] and plasmonic waveguiding.[173,174]

Several deposition methods have been employed to fabricate AgNW-based electrodes from NW solutions, such as spray-coating,[175–177] vacuum filtration followed by transfer,[62,178] Meyer rod coating,[80] and drop-casting.[164] Much progress has been made to develop AgNW-based transparent electrodes as a substitute for ITO.[88,89] For example, De et al.[178] achieved optical transmittance T = 85% and sheet resistance R_s = 13 Ω sq^{-1} on a PET substrate. Hu et al. reported AgNW networks with 8 Ω sq^{-1} and 80% diffusive transmittance in the visible range.[126] More recently, Leem et al.[179] reported $R_s \approx$ 35 Ω sq^{-1} at 98% transmittance. Scardaci et al.[176] demonstrated that AgNWs can be spray-deposited over a large area to form networks with T = 90% and R_s = 50 Ω sq^{-1}. AgNWs on a PET substrate have been reported to have good flexibility under bending[74,126,178] and good conductance against

Adv. Mater. 2015,
DOI: 10.1002/adma.201404446

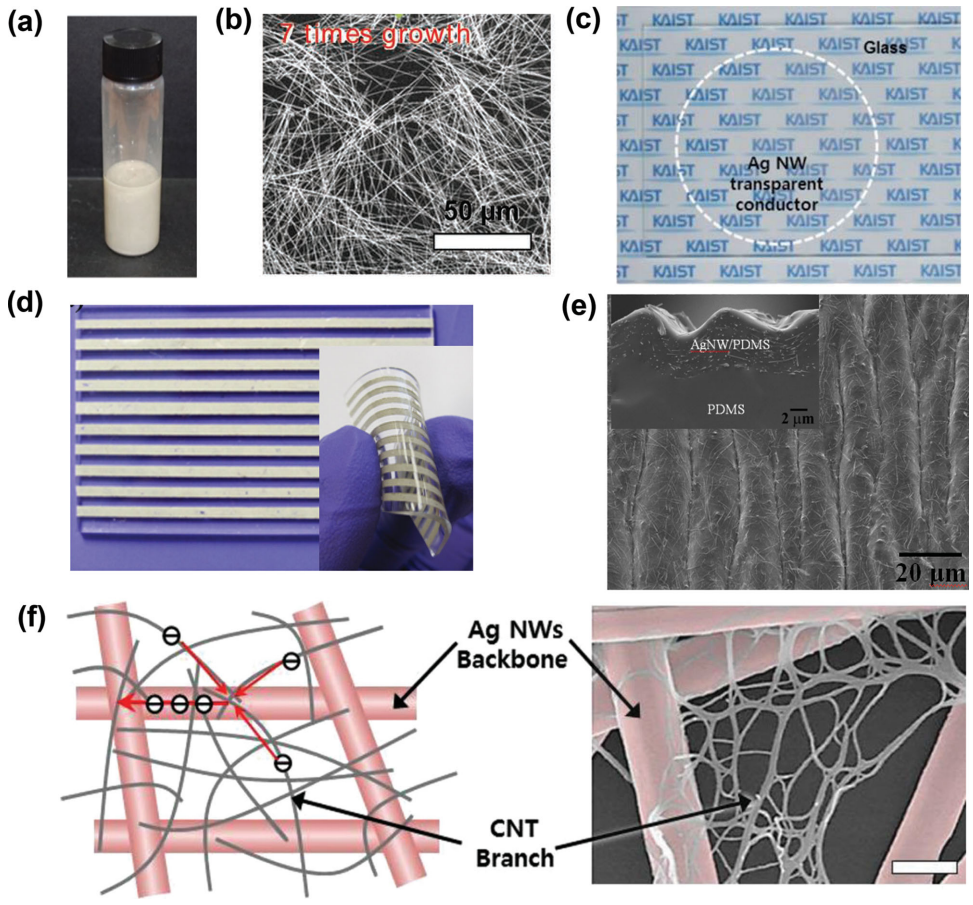

Figure 7. Very long Ag NWs fabricated by the SMG process: a) Digital image of the very long AgNW ink in ethanol. b) SEM images of AgNWs fabricated after 7 SMG steps. Scale bar: 50 μm. a,b) Reproduced with permission.[62] Copyright 2012, John Wiley and Sons. c) Image of a highly transparent conductor based on very long AgNWs on a glass substrate. Reproduced with permission.[76] Copyright 2012, Royal Society of Chemistry. AgNW/PDMS elastic conductors: d) The AgNW/PDMS elastic conductors with a linewidth of 800 μm patterned in parallel. The inset shows the conductors deformed by hand. e) SEM image of the buckled AgNW/PDMS surface after the stretching and releasing cycles. The inset shows the cross-sectional SEM image of the AgNW/PDMS layer. d,e) Reproduced with permission.[60] Copyright 2012, John Wiley and Sons. f) Schematic illustration (left) and SEM image (right) of multiscale AgNW/CNT hybrid structures with relatively larger dimension of AgNW backbone (pink colored) and smaller dimension CNT branch (gray-colored) for electron transport. The scale bar on right SEM image is 300 nm. Reproduced with permission.[106] Copyright 2014, John Wiley and Sons.

heat, water, acetone, and isopropyl alcohol (IPA) exposure.[126] Thanks to the superior optical/electrical performance and progress in the fabrication process, a wide range of flexible devices using AgNWs have been successfully demonstrated at low cost, including organic light-emitting diodes (LEDs)[180] shape-memory polymer LEDs,[181] and solar cells.[75,177,179,182]

With the strategies discussed in Section 2, AgNWs have also been explored recently as stretchable conductors. Pei's group embedded a AgNW network below the surface of several polymer matrices such as poly(acrylate),[69] PU,[118] and poly(tert-butylacrylate) (PtBA),[68] to form compliant electrodes. The addition of acrylic acid (AA) into the polymer composition of PtBA and poly(acrylate) play an important role, and improves the adhesion between the polymer and AgNWs, and thus ensures good transfer of the AgNWs into the polymer matrix. The fabricated electrodes were endowed with excellent compliance, high conductivity, and good transparency. A sheet resistance of 50.8 Ω sq^{-1} with transmittance of 90.2% and 7.5 Ω sq^{-1} with transmittance of 79.6% were achieved in AgNW–poly(acrylate) electrodes with 5% AA, and the sheet resistance increased by only 2.3 times at 50% strain.[69] The AgNW–PtBA composite with 5% AA showed a sheet resistance as low as 10 Ω sq^{-1} and remained conductive with a sheet resistance of 10^2–10^3 Ω sq^{-1} at a strain of 140%.[68] Alternatively, AgNWs were spray-deposited on a polydopamine-modified PDMS substrate, where the polydopamine layer rendered a highly hydrophilic surface to enhance the adhesion of AgNWs with PDMS.[40] The spray-deposited AgNWs demonstrated a low sheet resistance of 35 Ω sq^{-1} at 80% transmittance and good robustness against strain below ca. 15%. Recently, graphene oxide (GO) was introduced to solder the AgNW junctions, which greatly reduced the contact resistance, enhanced the stretchability and stability of AgNW networks.[73] Stretchable conductors prepared by coating GO-soldered AgNW networks with polyurethane acrylate (PUA) showed transmittance of 86.3% with a sheet resistance of 26 Ω sq^{-1} or 82.5% with a sheet resistance of 14 Ω sq^{-1}. The resistance was increased by 10.6 times under a tensile strain of 80%.

Very few studies have been reported for biaxially stretchable conductors. Ho et al. demonstrated biaxially stretchable conductors by transferring the AgNW network onto a biaxially prestrained (10%) PDMS substrate.[119] While the stable strain range was not very high (up to 5%), it was suggested that longer NWs could potentially increase the biaxial stretchability.

Despite the efforts that have been taken to make AgNW electrodes stretchable, most AgNW electrodes have showed increasing resistance with applied strain[68,69,73,80,118] or a small strain range for stable resistance (e.g., <20%),[40,119] which limits their applications as stretchable conductors. Recently, Xu and Zhu[60] demonstrated a promising approach to fabricate highly conductive and stretchable AgNW conductors by embedding the AgNW network just below the surface of PDMS, as shown in Figure 7d. The first several stretching and releasing cycles within a strain range of 80% rendered a constant conductivity of 5285 S cm^{-1} in a large range of tensile strain (0–50%). Figure 7e illustrates the underlying mechanism for the constant resistance under the large strain: the AgNW/PDMS layer formed a periodic wavy pattern after stretching/release, in contrast to the initial, flat surface. During stretching, the AgNWs slide between each other by overcoming the friction force; during release, the AgNWs cannot slide back, giving rise to the collective buckling of the top AgNW/PDMS layer and thus the wavy structure. Upon formation of the wavy structure, the conductor maintains a nearly constant resistance as no further NW sliding would occur during stretching.

Percolation theory predicts that the required NW density to keep the same conductivity dramatically decreases as the NW length increases, owing to the longer percolation paths and reduced NW junctions.[76] Effort has been devoted to manufacturing stretchable and transparent conductors with long NWs. Very long AgNWs prepared by seven reduction steps of $AgNO_3$ were vacuum filtrated and transferred onto a prestrained Ecoflex, followed by a thermal annealing process to remove the residue PVP and facilitate nanowelding between the NWs.[62] Transparent conductors with superior conductance (9–70 Ω sq^{-1}), transparency (90–96% on glass) and stretchability (highly conductive under strain up to 460%) were achieved. The same group later eliminated the annealing/welding process by using CNTs (with much smaller diameters of 1.2 nm and length of 2–10 μm) to promote the contact of the junction area and reduce the junction resistance.[106] As illustrated in Figure 7f, the addition of the CNTs improved the conductivity due to extra local conducting pathways and more firmly joined AgNWs junctions. The multiscale hybrid AgNW–CNT composite transferred to a prestrained Ecoflex substrate was able to accommodate tensile strain as high as 460%.

In addition to the 2D AgNW networks discussed above, hierarchical 3D assemblies with binary network structures were designed by Yu and co-workers[107,108] to enhance the electromechanical stability of AgNW-based stretchable conductors. One way is to dip-coat a PU sponge with a AgNW network, as shown in **Figure 8**a and b,[107] while the other way is to use oriented growth of ice to guide the assembly of the AgNWs into highly ordered micronetworks with interconnected compartmental units, as shown in Figure 8d and e.[108] PDMS has then been introduced to encapsulate the above 3D structures. Under strain, both the 2D AgNW network and the 3D structure (PU skeleton for PU–AgNW–PDMS conductors and AgNW compartmental micronetwork for 3D AgNW–PDMS conductors) can deform to accommodate the strain, leading to an improved electromechanical performance, as illustrated in Figure 8c and f, respectively. The PU–AgNW–PDMS conductors retained high conductivity (>19.2 S cm^{-1}) and a small increase in resistance under a tensile strain of 50%. For the AgNW compartmentalized architecture–PDMS conductor, the first stretching by 100% tensile strain led to a resistance increase of 150%. After that, little increase in resistance was observed for strains within 50%.

4.2. Copper Nanowires

Silver has a low natural abundance and AgNW-based electrodes are reported to be not cheaper than those based on ITO.[176,183] CuNWs thus become an appealing alternative due to the fact that copper has comparable conductivity to silver,[122] is low cost (1% the cost of silver), and is more abundant (1000 times than silver or indium).[128] CuNWs can be fabricated by a number of methods, including aqueous-based reduction of copper salts,[183–185] non-aqueous self-catalytic growth,[87] and electrospinning.[72,186] **Figure 9** shows CuNWs grown by several common methods. Much progress has been made to improve the performance of CuNW films, in terms of sheet resistance, transparency, and flexibility. With ultralong CuNWs and thus enhanced aspect ratio (Figure 9c), Zhang et al.[87] reported electrodes with a sheet resistance of ca. 90 Ω sq^{-1} at 90% transmittance. More recently, Guo et al.[78] demonstrated a sheet resistance of 51.5 Ω sq^{-1} at 93.1% transmittance with excellent flexibility. A nearly constant transmittance over the UV–vis–NIR range and a high ratio of electrical conductivity to optical conductivity (ca. 93) were achieved.[78,87]

Wu and co-workers[109] demonstrated that a CuNW network can reversibly slide on 3M VHB 4905 acrylic elastomer and serve as a compliant electrode for dielectric elastomer actuators. The CuNW network retains good conductivity at an area strain as high as 200%. Due to the fact that the transmittance changes during actuation, CuNW-based actuators can be used as light valves. CuNWs were also embedded with poly(acrylate)[122] and a PU matrix,[70] and the resistance increased with applied strain. 220 Ω sq^{-1} and 91.5% transmittance, or 5 Ω sq^{-1} and 70.5% transmittance were obtained for the poly(acrylate) matrix, while ca. 56 Ω sq^{-1} and 84.5% transmittance, or ca. 8 Ω sq^{-1} and 68.7% transmittance were obtained for the PU matrix. Pretreatment by 6-aminohexanoic acid can facilitate bonding between CuNWs and the PU matrix, suppress the sliding of the CuNWs during stretching, and hence improve the stretchability. Although the resistance increased with applied strain, the resistance can be kept below 100 Ω sq^{-1} for strains of up to 60%.[70]

The stretchability was significantly improved in a plasmonic nanowelded CuNWs network that was transferred onto Ecoflex.[63] Fast and localized plasmonic heating and welding at the NW junctions was performed through a polarized laser to reduce the resistance, which avoided oxidation of the CuNWs during traditional bulk heating and damage to the substrate materials. The resulting CuNW/Ecoflex can be stretched to

Adv. Mater. 2015,
DOI: 10.1002/adma.201404446

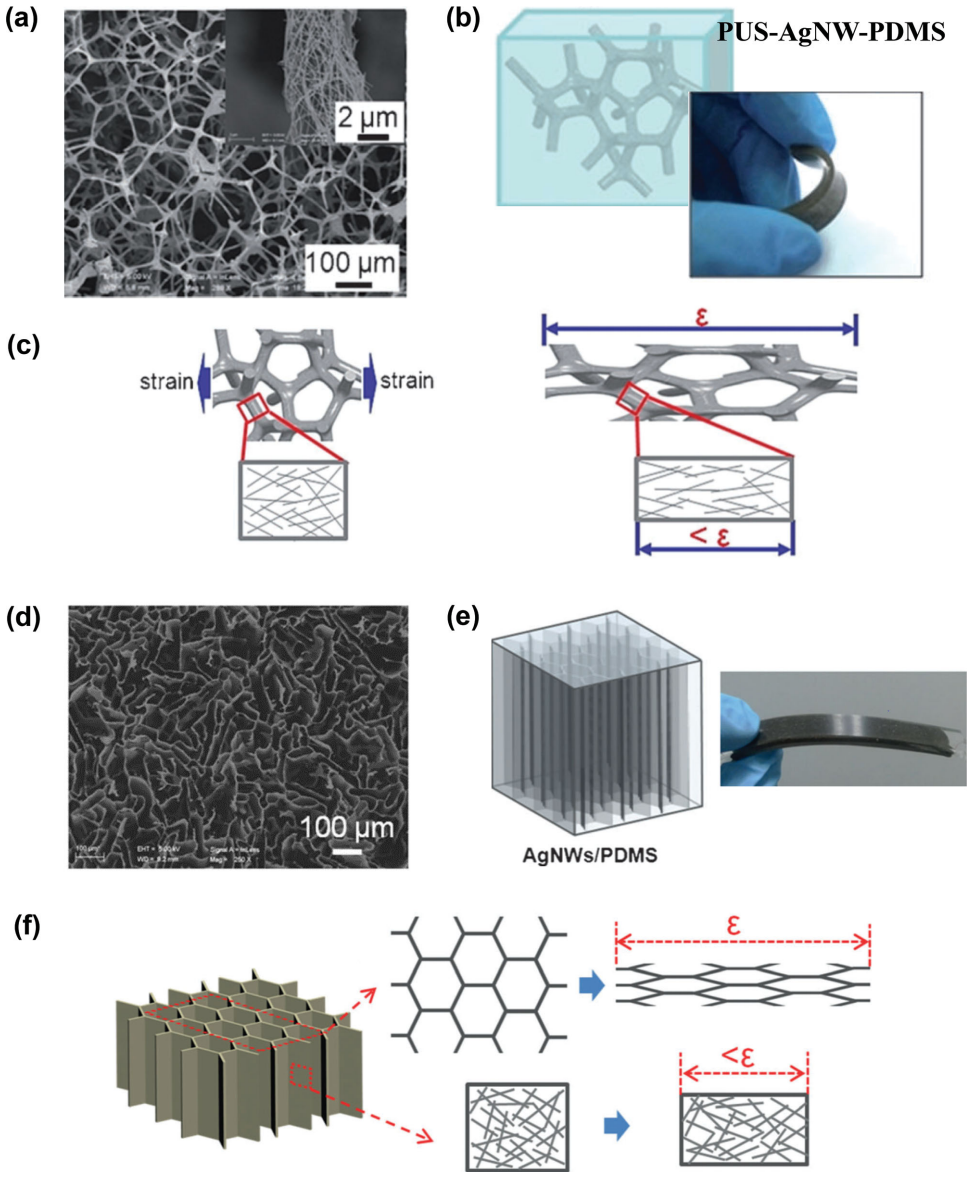

Figure 8. Stretchable conductors with 3D hierarchical structures. PUS–AgNW–PDMS stretchable conductors: a) SEM image of PUS–AgNW before introducing PDMS. b) Schematic (left) and photograph (right) of PUS–AgNW–PDMS composite. c) Schematic illustration of the deformation of the PUS–AgNW–PDMS conductors during stretching. Both the 3D PU micro-network and the 2D AgNW (on the surface of PU) nano-network deform to absorb the strain. a–c) Reproduced with permission.[107] Copyright 2013, John Wiley and Sons. AgNW compartmental architectures-PDMS stretchable conductors: d) SEM image for 3D AgNW compartmental architectures with 25 mg cm^{-3} of AgNWs before introducing PDMS. e) Schematic (left) and photograph (right) of 3D AgNW–PDMS composite. f) Schematic illustration of the deformation of the AgNW–PDMS conductors during stretching. Both the 3D compartmental micro-network and the 2D AgNW nano-network deform to absorb the strain. d–f) Reproduced with permission.[108] Copyright 2014, John Wiley and Sons.

250% strain with slow resistance change with strain. Very recently, CuNW-based conductors with stable conductivity during strain were achieved by a CuNW–poly(vinyl-alcohol) (PVA) aerogel embedded with PDMS (Figure 9d and e), where the addition of a trace amount of PVA stabilized the CuNW scaffolds and maintained the structural integrity during both the fabrication process and mechanical pressing/stretching.[110] The highly porous structure introduced through the freeze-drying process enabled CuNW–PVA–PDMS ambers to endure a compressive strain of 60% and a tensile strain of 60%. No particular resistance change was observed after several cycles of stretching, as shown in Figure 9f.

Electrospinning or electrostatic spinning offers a simple and versatile route to draw continuous NWs, often called ultrathin fibers (with diameters ranging from a few micrometers down to a few nanometers) from solution or a melt.[187] This process is widely used to generate numerous types of polymer fibers and polymer composites.[188–190] Electrospun sub-micrometer Cu fibers or NWs have been reported[186] where copper nitride or copper acetate were used as the precursor and polyvinylbutyral

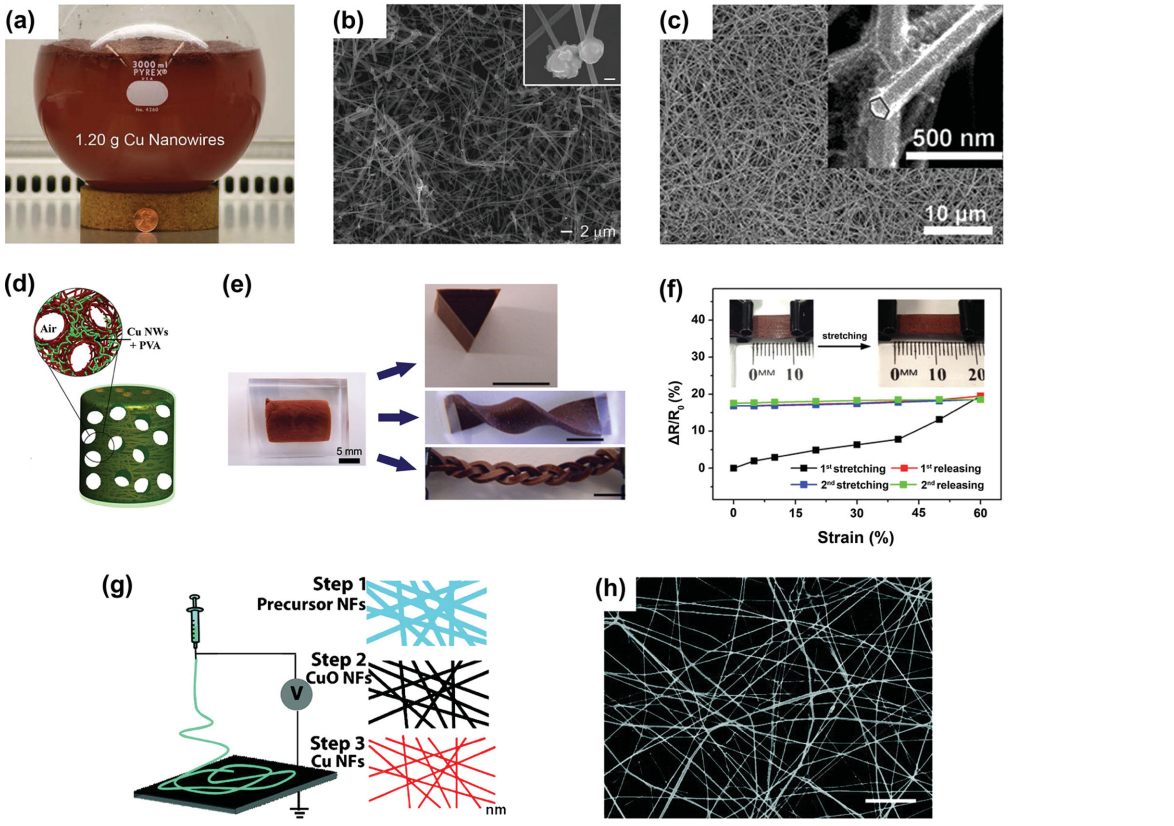

Figure 9. a) An image showing as-grown CuNWs in reaction flask by reducing $Cu(NO_3)_2$ with hydrazine. b) SEM image of CuNW products in (a) with nanowires of 90 ± 10 nm and length of 10 ± 3 μm. One end was attached with copper particle as shown in the inset (scale bar: 200 nm). a,b) Reproduced with permission.[183] Copyright 2010, John Wiley and Sons. c) Self-catalytic grown single crystalline ultralong copper nanowires with excellent dispersibility. The average diameter was ca. 78 nm and lengths were tens to hundreds of micrometers and even several millimeters. Reproduced with permission.[87] Copyright 2012, American Chemical Society. d) Schematic illustration of CuNW–PVA aerogel before PDMS embedding. e) Left: Photograph of the CuNW–PVA–PDMS rubber amber. Right: The rubber ambers could be cut-shaped into 1D, 2D, and 3D structures. Scale bars: 1 cm. f) Resistance of the CuNW–PVA–PDMS rubber amber as a function of tensile strain up to 60%. d–f) Reproduced with permission.[110] Copyright 2014, American Chemical Society. g) Schematics showing setup (left) and fabrication steps (right) for electrospinning of Cu nanofibers. h) SEM image of electrospun Cu nanofibers with diameters of ca. 100 nm. Scale bar: 10 μm. g,h) Reproduced with permission.[72] Copyright 2010, American Chemical Society.

or PVA were used as the matrix to generate composite fibers, followed by thermal treatment to form copper oxide fibers. After hydrogen reduction, these copper oxide fibers could be reduced into copper fibers. Wu et al.[72] fabricated continuous Cu nanofibers with a length of more than 1 cm and a diameter of ca. 100 nm (Figure 9g and h). A low sheet resistance of 50 Ω sq^{-1} at a high transmittance of 90% was obtained as a result of the ultrahigh aspect ratio (up to 100 000) and fused junctions between the Cu nanofibers. The Cu nanofibers on PDMS showed good robustness against bending to a 6 mm radius of curvature and stretching to 10% strain.

Despite the relatively low cost and high performance, the poor stability against thermal oxidation and chemical corrosion of CuNWs and the resulting degraded conductivity over time may hamper their applications. Several ways are being explored to improve the long-term stability without sacrificing much of the conductivity and transparency, such as coating with an aluminum-doped zinc oxide (AZO)/aluminum oxide (Al_2O_3) passivation layer,[191] coating with nickel,[192] coating with graphene oxide platelet,[193] embedding the materials underneath poly(acrylate),[122] and treating them with hydrogen plasmas.[87]

5. Graphene-Based Stretchable Conductors

Since the first preparation of highly oriented pyrolytic graphite by mechanical exfoliation,[194] graphene has become of central interest due to its unique two-dimensional structure with atomically thin carbon atoms arranged in a honeycomb lattice, and its unique properties, including excellent electron mobility, high chemical and thermal stability, ultrahigh strength, large specific surface area, and low contact resistance with organic electronic devices.[195–198] A myriad of applications have been demonstrated, such as electrochemical sensors and biosensors, polymer composites, field-effect transistors and organic electronic devices, and energy conversion and storage devices.[195,199–208] For these applications, large-scale synthesis and assembly of graphene pose a major challenge.[209] Various methods have been developed including epitaxial growth on SiC[210,211] and metal surfaces,[212] reduction from graphite oxide,[213–215] liquid-phase exfoliation,[216,217] and CVD,[218,123] among which CVD is relatively simple and can produce large-area, high-quality graphene. After growth, the graphene can be

Adv. Mater. 2015,
DOI: 10.1002/adma.201404446

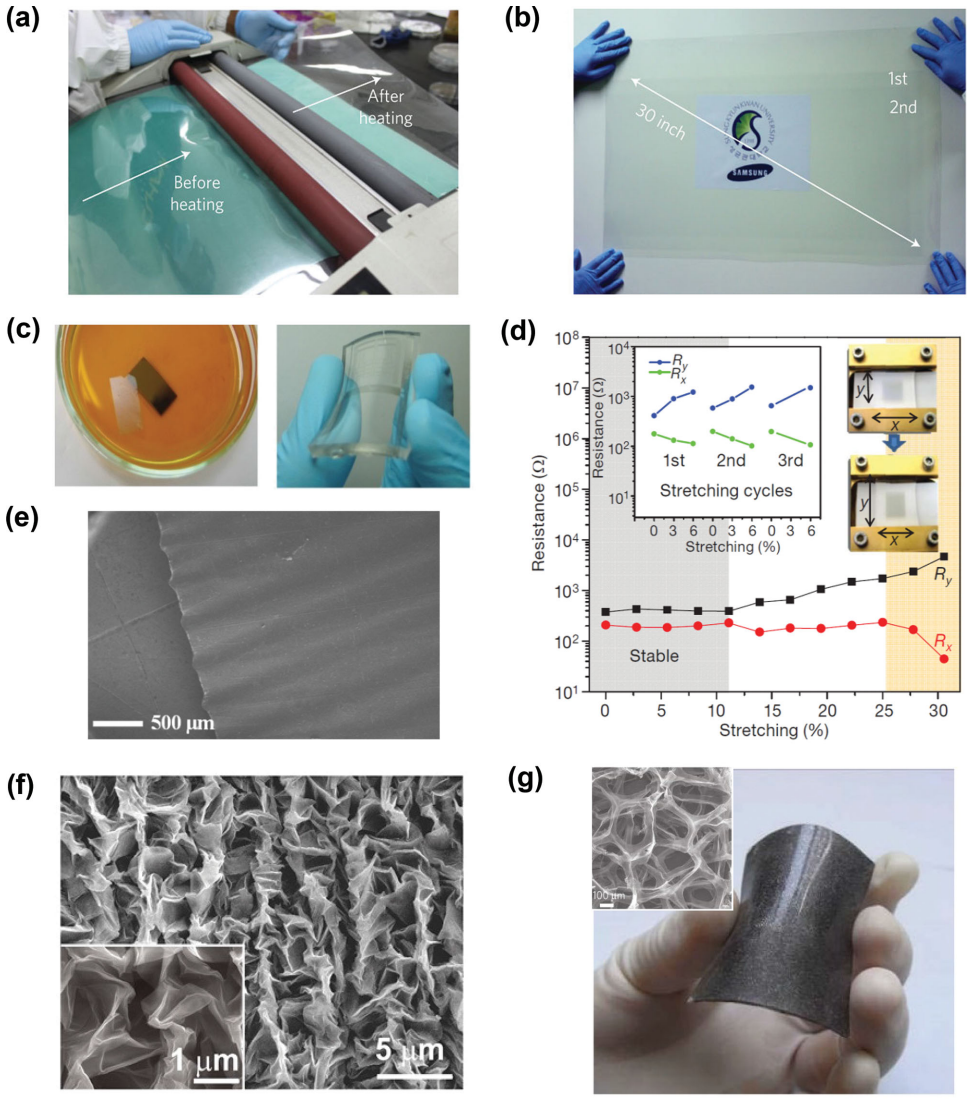

Figure 10. a) Roll-to-roll transfer of graphene films from a thermal release tape to a target substrate (PET film). b) A 30-inch multilayer graphene film transferred onto a 35-inch PET sheet. a,b) Reproduced with permission.[224] Copyright 2010, Nature Publishing Group. c) Left: Graphene films floating in solution after etching the nickel layers. Then the floating graphene film can be transferred by direct contact with substrates. Right: Graphene films on the PDMS substrate. d) Resistance vs. tensile strain for a graphene film transferred to PDMS substrate isotropically prestrained by 12%. The left inset shows the results for the graphene film transferred to an unstretched PDMS substrate. The right inset shows the stretching process. c,d) Reproduced with permission.[123] Copyright 2009, Nature Publishing Group. e) Top view SEM image of the wavy/wrinkled graphene on PDMS support. Reproduced with permission.[124] Copyright 2014, American Chemical Society. f) Crumpled graphene film generated by sequentially relaxing the substrate along two pre-stretched direction. Reproduced with permission.[111] Copyright 2013, Nature Publishing Group. g) Photograph of a GF/PDMS composite under bending. Inset: SEM image of a freestanding GF with ultralow density. Reproduced with permission.[65] Copyright 2011, Nature Publishing Group.

transferred onto arbitrary substrates with the assistance of PDMS,[123,111] poly(methyl methacrylate) (PMMA),[219–221] or thermal release tape.[222–224] Bae et al. reported thermal-release-tape-assisted roll-to-roll transfer of 30-inch CVD-grown graphene films onto flexible PET substrates, as indicated in **Figure 10**a and b.[224] The transferred graphene films showed a high quality and a half-integer quantum Hall effect. A sheet resistance of ca. 30 Ω sq^{-1} at ca. 90% transmittance was achieved for p-doped four-layer graphene films.

5.1. Graphene

The transmittance of graphene is dependent on the number of layers with 2.3% light absorption for each layer of graphene over the visible range.[225] The electrical conductivity, however, strongly relies on the crystalline quality and surface morphology (uniformity, defects, etc.).[195] The high transparency and good conductivity make graphene a promising candidate as transparent electrodes.[226–228] Kim et al. reported large-scale, patterned synthesis of high-quality graphene using

the CVD method and effective transfer of graphene to different substrates by etching the nickel substrate on which the graphene was synthesized (Figure 10c).[123] A sheet resistance of ca. 280 Ω sq^{-1} and a transmittance of ca. 80% were achieved, where UV/ozone thinning was adopted to improve the transmittance. To enhance the electromechanical stability, the graphene film was transferred to biaxially prestrained PDMS (ca. 12% strain). After releasing the PDMS, both longitudinal and transverse resistance remained stable within 11% tensile strain, and increased by one order of magnitude at ca. 25% strain, as shown in Figure 10d. An alternative way to render the graphene film stretchable is to grow the graphene on wavy Cu foil instead of the planar one, followed by drop-casting PDMS and etching the Cu foil (Figure 10e).[124] The resulting graphene/PDMS exhibited transmittance between 50% and 60%. Another coating of PVA on top of the graphene greatly suppresses the formation of cracks during stretching and thus enhanced the stretchability. The resistance of graphene/PDMS coated with PVA increased by ca. 2 times under tensile strain of 40%.

By sequentially releasing the biaxially prestrained VHB 4905 substrate with a graphene film on top along the two prestrain directions, self-organized, crumpled hierarchical structures can be formed, as shown in Figure 10f.[111] When stretching the substrate back in both directions, the crumpled structure can be "unfolded". With unequal prestrains of 10% and 500%, the crumpled graphene conductor can accommodate an extreme strain of 450% along the direction with the higher prestrain. Interestingly the crumpled graphene is superhydrophobic. The reversible crumpling–unfolding process can be used to tune the wettability and optical transmittance of the graphene.

Macroscopic 3D graphene foams (GFs) were synthesized by a template-directed CVD process using nickel foam as the template.[65] Owing to the well-interconnected 3D conducting network, the GF/PDMS composite with low graphene loading of ca. 0.5 wt% showed good conductivity of ca. 10 S cm^{-1} and high fracture stain of ca. 95% (Figure 10g). After being treated by five cycles of stretching, the resistance increased ca. 30% under 50% tensile strain.

5.2. Graphene-Based Hybrid Structures

Undoped graphene typically shows poor electrical conductivity owing to poor crystal quality, structural defects, or large interlayer resistance,[195] which restricts its application as a conductor. In order to enhance the conductivity, methods such as chemical doping[84,229–232] and introducing CNTs[233] and metal nanostructures (e.g., depositing on top of graphene or mixing with graphene)[83,234–236] have been developed. Graphene–Ag hybrid fibers were fabricated by wet-spinning process and subsequent chemical reduction, and they exhibited enhanced conductivity and current capacity.[83] For Ag-doped graphene fibers transferred onto PDMS prestrained by 150%, the conductivity was maintained for strains within 150%. In recent work, Lee and co-workers increased the conductivity of graphene films by spin-coating a thin layer of AgNW network (**Figure 11**a) on top, where the conducting pathways of the graphene and AgNWs function complementary to each other, and a high resistance at defect areas in the graphene was circumvented (Figure 11b).[125] Consequently, a low resistance of 33 Ω sq^{-1} at a high transmittance of 94% was achieved. Graphene–AgNW on PDMS (Figure 11c) exhibited a large strain tolerance of 100% with negligible resistance degradation (Figure 11d); in addition, the hybrid structure showed a much higher breakdown electric field and better stability against thermal oxidation compared with pure AgNWs.

6. Metal-Nanoparticle-Based Stretchable Conductors

In addition to 1D nanotubes/NWs and 2D graphene, efforts have also been made to employ 0D metal NPs, such as silver NPs (AgNPs),[237,238] copper NPs,[239,240] and gold NPs (AuNPs),[241] to develop conductors. Stretchable conductors have been realized by combining wavy structures and/or polymers with metal NPs, especially AgNPs. It is of note that NPs are often ink-jet printed, which offers a low cost, eco-friendly,

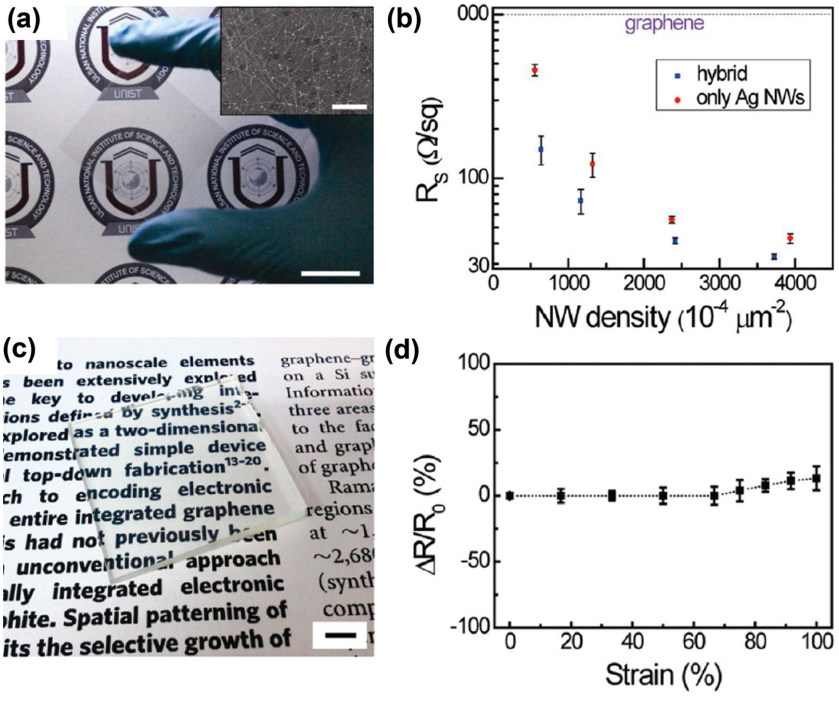

Figure 11. Graphene–AgNW hybrid conductors: a) Photograph (scale bar: 2 cm) and SEM image (inset, scale bar: 5 μm) of graphene–AgNW hybrid film on a PET substrate. b) Sheet resistance of silver nanowires, graphene and hybrid structures at different NW densities. c) A photograph of graphene–AgNW hybrid film on a PDMS substrate. Scale bar: 5 mm. d) Relative resistance change under various tensile strains. Reproduced with permission.[125] Copyright 2013, American Chemical Society.

DOI: 10.1002/adma.201404446

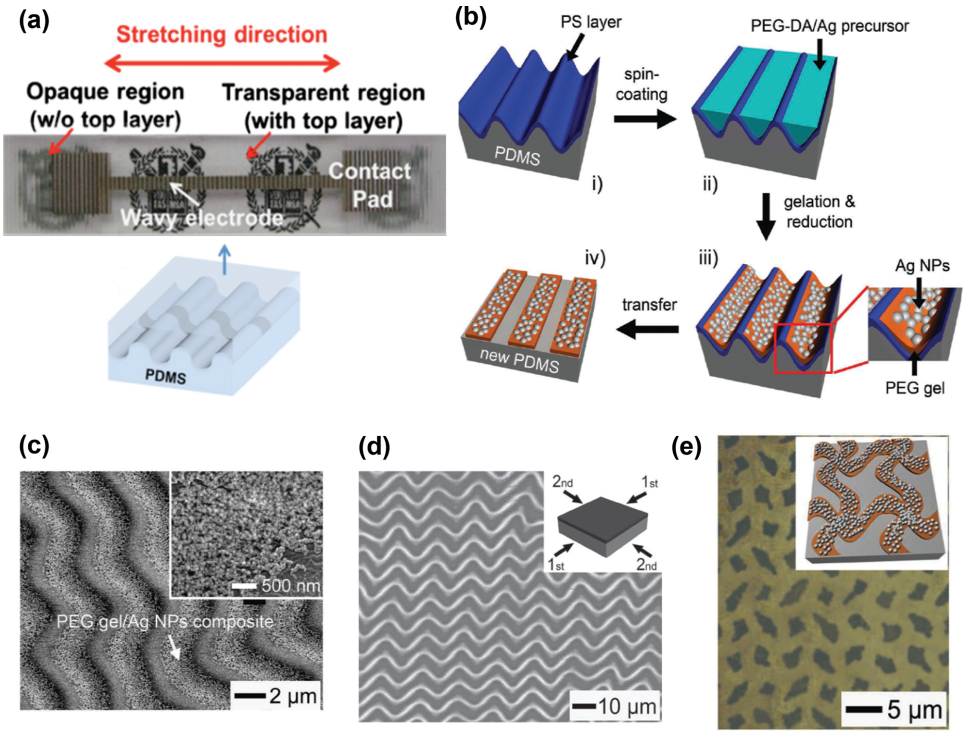

Figure 12. a) Schematic (bottom) and optical image (top) of the inkjet-printed AgNPs based stretchable conductor. Reproduced with permission.[113] Copyright 2011, AIP Publishing LLC. AgNP–polymer composites with ordered zigzag patterns for stretchable conductors: b) Schematics showing the fabrication process. c) Low and high (inset) magnification SEM images of the polymer gel and AgNPs composites inside the trenches. d) Schematic (inset) and image of the ordered zigzag patterns formed by successively releasing the 2D strains. e) Schematic (inset) and optical image of the biaxially stretchable conductor by transferring the zigzag patterns successively in a perpendicular configuration. b–e) Reproduced with permission.[121] Copyright 2011, John Wiley and Sons.

and convenient way to fabricate stretchable conductors. Chung et al. developed a stretchable conductor by ink-jet printing AgNPs onto a PDMS substrate with a wavy, roughened surface.[113] The wavy, roughened surface can improve the stretchability owing to two features: i) it promotes the adhesion of the ink, and ii) it helps release the stress in the Ag film during stretching. Another layer of PDMS was covered on top of the printed AgNP line to further improve the electromechanical stability. For tensile strains up to 30%, the resistance increased less than three times. A schematic and an optical image of the fabricated conductor are presented in **Figure 12**a. Hyun et al.[121] used the buckled polymer as a template to create AgNP-based stretchable conductors with wavy structures. The fabrication flow is shown in Figure 12b. The polystyrene (PS)-coated PDMS was buckled by applying thermal or mechanical strain (i) and then the trench was filled with polymer gel and metal precursors (ii). After UV exposure to crosslink the polymer, and chemical reduction of the metal precursor into the AgNPs, AgNP–polymer composites were formed and patterned (iii). Figure 12c shows an SEM image of the polymer-gel–AgNP composite inside the trench. Following that, the composite patterns were transferred onto another PDMS substrate (iv). If the 2D strain of the PS-coated PDMS is released sequentially, ordered zigzag patterns can be generated, as shown in Figure 12d. The AgNP conductors with zigzag patterns exhibited large conductivity (ca. 10^4 S cm^{-1}) within the tensile strain range of 0–50%. Biaxially stretchable conductors with biaxial stretchability of 40% were fabricated by transferring two zigzag patterns successively, as shown in Figure 12e.

Besides introducing wavy patterns to develop AgNP-based stretchable conductors, stretchable conductors can be fabricated by creating conductive composite mats of AgNPs and electrospun poly(styrene-*block*-butadiene-*block*-styrene) (SBS) rubber fibers.[112] The composite mats were generated by first dipping SBS fibers in a $AgCF_3COO$ precursor solution and then reducing the precursor into AgNPs. AgNPs can be found in the interior and on the surface of the fibers. The AgNPs formed the solid shell on the surface of the fibers and upon stretching; the AgNP shells began to rupture at a low strain. Both the electron pathways from the interconnected AgNPs inside the fiber and the ruptured silver shell pieces connecting the fibers contributed to the conductivity of the composite mat. For the composite mat with a thickness of 150 μm, a high conductivity of 5400 S cm^{-1} was achieved. The conductivity decreased to ca. 2200 S cm^{-1} under a tensile strain of 100%, and to 610 S cm^{-1} under tensile strain of 140%.

A high conductivity and high stretchability were also achieved in AuNP–PU composites, where citrate-stabilized AuNPs with a diameter of ca. 13 nm were used as the filler, and PU was used as the polymer matrix.[114] Two fabrication methods, layer-by-layer (LBL) deposition and vacuum-assisted flocculation (VAF) were used to fabricate the composite films. The initial conductivity of a 5× LBL stack (laminated five sheets of free-standing LBL composite film) and a 5× VAF stack composite was

11 000 S cm^{-1} and 1800 S cm^{-1}, with maximum strains of 115% and 486%, respectively. The conductivity decreased to 3500 S cm^{-1} for 5× LBL and 210 S cm^{-1} for 5× VAF at 60% tensile strain and 2400 S cm^{-1} and 94 S cm^{-1} at 110% tensile strain, respectively. The extraordinary electromechanical performances can be ascribed to the stress-induced NP organization. The AuNPs self-organized into 3D cellular networks under tensile strain, due to the local phase separation of the AuNPs in the polymer. Owing to the existence of stress-induced cellular networks, the percolation threshold for the composite decreases and thus the conductivity is larger compared to the composite with the same volumetric fraction of the filler but without the self-organized networks.

7. Device Applications

In the previous sections, we have reviewed recent progress in developing new materials and structures for stretchable conductors based on CNTs, metallic NWs, graphene, and metallic NPs. Imparted by the excellent mechanical compliance and high electric conductivity, these stretchable conductors can be integrated with other materials and structures to form stretchable devices and systems. In this section, we will summarize the recent efforts on this front.

7.1. Stretchable Interconnects

A straightforward application of stretchable conductors is stretchable interconnects that can be used to connect rigid device components, following the 2nd architecture mentioned in the Introduction. In representative work, SWNT pastes and conductors were used as interconnects for an array of organic transistors to form a 19 × 37 organic-transistor-based stretchable active matrix.[50] The interconnects did not influence the characteristics of the transistors and the active matrix showed negligible and recoverable change in electrical behavior after 30 stretching/release cycles for up to 70% strain. The stretchable interconnects have been widely used in stretchable LED systems where stretchable conductors connect and illuminate the rigid LED elements. The LEDs function well when the systems are stretched,[37,41,53,60,101,102,107,121] twisted,[53,119] or folded.[53,60] Sekitani et al. developed a 16 × 16-pixel rubber-like stretchable active-matrix display composed of 16 × 16 driving cells, organic LEDs and elastic electrical interconnects (wirings) based on a printable SWNT-rubber composite.[47] The highly conductive and stretchable conductors essentially absorbed most of the strain during stretching (30–50%), folding, and crumpling. The driving cell and organic LEDs experienced little strain, and thus the electrical and mechanical functions of the display system were maintained (**Figure 13**a). In another example, the potential of the transparent and stretchable graphene–AgNW hybrid conductors in wearable electronics was demonstrated. A see-through single-pixel contact-lens display was fabricated, where the inorganic LED (ILED) was integrated onto a soft and curved contact lens by using a graphene–AgNW hybrid conductor as the conformal electrical interface (Figure 13b).[125] The device was further studied in vivo by fitting it on a live rabbit eye. Using the stretchable interconnects to wire rigid device elements renders the otherwise rigid systems stretchable. The enhanced stretchability makes it possible for these systems to integrate onto arbitrary, even dynamic surfaces[47] and sustain large deformations, including stretching, bending, twisting, and folding, greatly expanding their application scope.

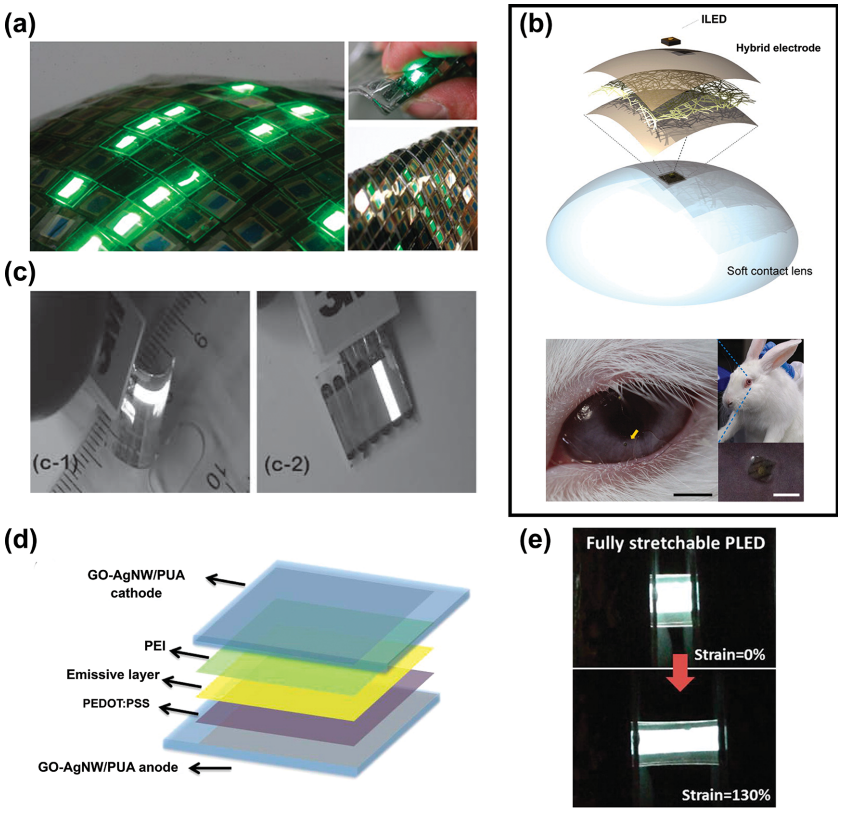

Figure 13. a) Images of a large-area stretchable display consisting of a driving-cell active matrix and organic LEDs integrated by printed CNT elastic conductors. The stretchable display can be spread over arbitrary curved surfaces and exhibit excellent durability under folding and crumpling. Reproduced with permission.[47] Copyright 2009, Nature Publishing Group. b) Top: Schematic illustration of the single-pixel contact lens display integrating an ILED on wearable eye contact lens using the graphene–AgNW hybrid electrode as the conformal electrical interface. Bottom: A photograph of the ILED-hybrid electrode-contact lens device on a rabbit eye. The right bottom inset shows the ILED part of the device. Scale bars: 5 mm (black), 300 μm (white). Reproduced with permission.[125] Copyright 2013, American Chemical Society. c) Photographs of shape memory PLEDs emitting light when bent with a radius of 2.5 mm (left) and recovered to flat shape after heating (right). Reproduced with permission.[181] Copyright 2010, John Wiley and Sons. d) Schematics of stretchable PLED, where GO soldered-AgNW/PUA composite were used as both anode and cathode. e) Optical photographs of a fully stretchable PLED emitting white light at relaxed and strained states. d,e) Reproduced with permission.[73] Copyright 2014, American Chemical Society.

Adv. Mater. **2015**,
DOI: 10.1002/adma.201404446

7.2. Stretchable Polymer Light-Emitting Devices

Polymer light-emitting devices with an emissive polymer layer sandwiched by two highly flexible/stretchable, transparent and conductive electrodes have been demonstrated. AgNW–polyacrylate (as anode) and SWNT–PtBA (as both anode and cathode) electrodes have been used to fabricate polymer light-emitting devices.[67,181] Embedding the AgNWs or SWNTs into polymer matrices leads to conductors with good mechanical robustness and low surface roughness. These nanomaterial-polymer composite electrodes introduce new features to polymer light-emitting devices: i) they can be deformed into various temporary or stable shapes, owing to the use of shape-memory polymers like PtBA and polyacrylate; ii) compared with LEDs using non-stretchable electrodes, the high flexibility of the AgNW–polyacrylate electrodes and the high stretchability of the SWNT–PtBA electrodes allow for large-strain deformations during bending with 8% tensile/compressive strain (for AgNW–polyacrylate-electrode-based devices, Figure 13c) or stretching up to 45% strain (for SWNT–PtBA-electrode-based devices) without losing much of the electroluminescent properties. Recently, Liang et al. introduced PUA-embedded AgNW percolation networks with junctions soldered by graphene oxides as both the anode and cathode to fabricate fully stretchable white polymer LEDs (Figure 13d).[73] As a result of the high stretchability and conductivity, the LEDs were stretched up to 130% strain without losing their functionality, as shown in Figure 13e.

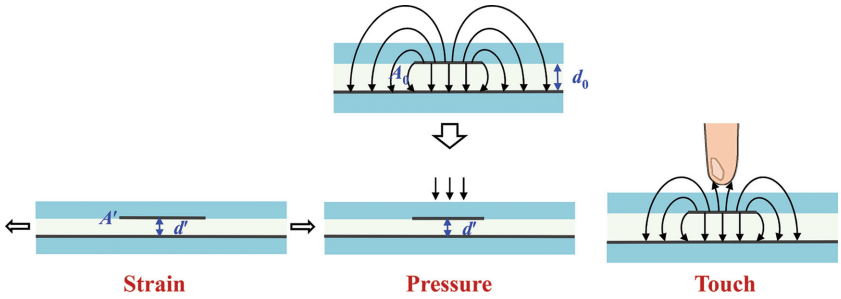

Figure 14. Schematic illustrations showing the mechanisms of capacitive strain, pressure and touch sensing: the initial state (top), under strain (bottom left), under pressure (bottom middle) and under finger touch (bottom right). A_0, d_0 and A', d' represent the overlapped area of the electrodes and the separation between electrodes for the initial state and under the stimuli, respectively. Reproduced with permission.[242] Copyright 2014, Royal Society of Chemistry.

7.3. Stretchable Capacitive Sensors

Two conductors with a dielectric layer sandwiched in between form a parallel-plate capacitor whose capacitance changes as a result of dimensional change, change in the dielectric constant, or change in the surrounding electric field, which forms the basis of many multifunctional sensors, such as strain, pressure, and touch sensors in response to planar strain, normal pressure, or finger touch, respectively.[242] Despite the viscoelasticity of the polymer matrix and the friction between the nanomaterials and the polymer matrix under deformation, stretchable capacitive sensors typically exhibit low hysteresis, fast response, and good durability, and are less susceptible to overshooting and stress relaxation.[130,243] A number of capacitive sensors based on CNTs or AgNWs conductors have been reported.[39,60,130,118,242–245]

As shown in **Figure 14**, when a tensile in-planar strain (ε) is applied to a parallel-plate capacitor with the initial overlapped length l_0, width w_0, and separation d_0 between the electrodes, the electrode length increases to $(1+\varepsilon)l_0$, the width decreases to $(1-\nu_{\text{electrode}}\varepsilon)w_0$, and the separation decreases to $(1-\nu_{\text{dielectric}}\varepsilon)d_0$ due to the Poisson effect. Considering both the electrodes and dielectrics are mainly composed of polymers, we can assume their Poisson ratios to be 0.5; thus, under small strain the capacitance under tensile strain is given by:

$$C=\varepsilon_0\varepsilon_r\frac{(1+\varepsilon)l_0(1-\nu\varepsilon)w_0}{(1-\nu\varepsilon)d_0}=\varepsilon_0\varepsilon_r\frac{(1+\varepsilon)l_0w_0}{d_0}=(1+\varepsilon)C_0 \quad (6)$$

where ε_0 and ε_r represent the electric constant and dielectric constant for the dielectric layer, respectively, C_0 represents the initial capacitance. In theory, the capacitance change has a linear relationship with tensile strain. The gauge factor, defined as the relative change in capacitance divided by the mechanical strain, is calculated to be $GF=\Delta C/C_0\varepsilon=1$. AgNWs embedded below the surface of PDMS,[60,242] AgNWs embedded below the surface of PU,[118] percolating CNTs networks encapsulated inside PDMS,[243] buckled CNTs on top of PDMS,[39] CNTs film embedded inside PDMS or Dragon skin,[130] micro contact printed CNT-doped PDMS[245] and in situ polymerized PU/MWNT elastomer[246] have been used to construct stretchable capacitors. PDMS,[60,130] Ecoflex,[39,242,245] Smooth-on Dragon skin,[130] and 3M tapes[118] are the common choices for the dielectrics. As a result of the fringing fields associated with finite-size parallel-plate capacitors,[243] the reported gauge factors were generally less than the theoretical value. The sensors exhibited good linearity and stability with ther gage factors ranging from 0.4[39] to 1.[60] The stretchability of 50%[39,60,242] to 100%[130,243] was demonstrated using highly stretchable conductors. Such highly stretchable strain sensors are ideal for wearable electronics, human motion detection, rehabilitation, robot systems, and other applications, where the strain range far exceeds the detecting range of conventional metal-foil strain sensors (gauges). The wearability and large-strain sensing capability were demonstrated in monitoring various human motions (**Figure 15**a–c) [130,242] and in a typical robotic linkage.[243]

Similarly, capacitive sensors can respond to an applied pressure due to the decreased distance between the two electrodes (Figure 14, bottom middle), also resulting in an increase in capacitance. By placing orthogonally patterned stretchable conductor lines, a grid of stretchable capacitors was fabricated, capable of measuring the pressure applied on each pixel (i.e., pressure mapping) (Figure 15d).[39] The sensitivity of the pressure sensor depends on how "compliant" the dielectric layer is. A high sensitivity of 3.3 kPa^{-1} was achieved with a highly porous Scotch Tape as the dielectric.[118] Crosstalk (the influence of the applied pressure on the adjacent pixels[39]) is a challenge for such pressure-sensor arrays. Fortunately, since the stretchable materials are generally very compliant, these

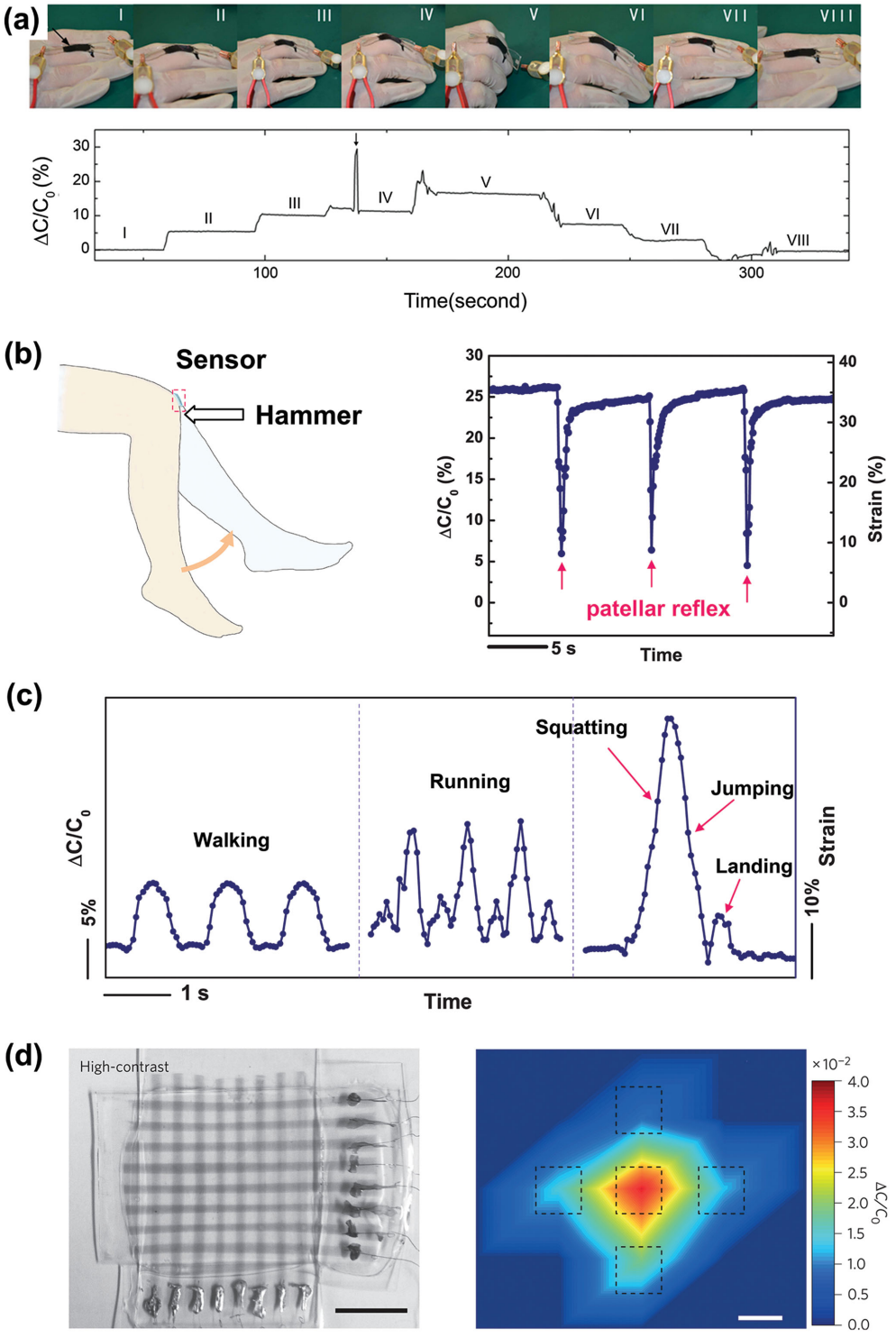

Figure 15. a) Still pictures of the prototypical data glove (top) integrating a CNT-based capacitive strain gauge onto a rubber glove and corresponding capacitive responses (bottom) when gradually folding (I–V) and then unfolding (VI–VIII) the fingers. The arrow in the bottom image in (a) indicates an accidental disruption of the copper wire. Reproduced with permission.[130] Copyright 2013, Nature Publishing Group. Demonstrations showing the large-strain sensing capability for capacitive sensors based on AgNW–PDMS stretchable conductors: b) Schematic showing the patellar reflex experiment (left) and capacitance change/strain caused by knee motion in patellar reflex (right). c) Relative capacitance change and strain versus time for various human motions. b,c) Reproduced with permission.[242] Copyright 2014, Royal Society of Chemistry. d) Photograph of the CNT based capacitive pressure sensor array with enhanced contrast (left) and the pressure profile indicated by capacitance change when 1 MPa pressure was applied on the central pixel (right). Scale bar: 1 cm (left,black), 2 mm (right, white). Reproduced with permission.[39] Copyright 2011, Nature Publishing Group.

Adv. Mater. **2015**,
DOI: 10.1002/adma.201404446

stretchable pressure sensors exhibited much lower cross-talk than those fabricated out of non-stretchable polyester films.[39,247]

The same capacitor configuration can be used for touch sensing as well. Different from strain and pressure sensors, the mechanism of capacitive touch sensors is based on disturbing the fringing electric field by a finger (Figure 14, bottom right). The fringing electric field of the sensor can be disturbed as long as a finger or other grounded conducting medium is in proximity, leading to a long sensing range. In addition, the sensor can be used in both pressing mode and proximity mode, and the capacitance changes are dominated by the interacting area and the distance between the finger and the sensor.[242] AgNW based stretchable touch sensors with interdigitated and diamond-shaped patterns were demonstrated by Cui et al.[244]

The capacitive sensors described above are mechanically compliant, simple in fabrication, and it is easy to integrate several functions into one device.[118,242] The sensor can function well when more than one stimulus is present: the gauge factor for the strain sensor was found to be unchanged when touched. At the same time, the performance of the pressure sensor remained nearly the same when stretched.[118] Their high sensitivity, good stretchability, and multifunctionality make capacitive sensors an excellent choice for artificial skins for robots and prosthetic devices, touch panels, and wearable smart devices. Transparency can also be imparted onto capacitive sensors,[39,130,118] so that the sensor can be incorporated into optoelectronic devices, such as solar cells and mechanically robust displays.

7.4. Electroactive Polymer Actuators

Stretchable conductors can be used in actuators as well. An electroactive polymer (EAP) actuator consists of two stretchable electrodes (conductors) and an EAP layer sandwiched in between. Note that for EAP actuators the electrodes are often called compliant electrodes. EAP actuators change shape (thinner in thickness and larger in area) in response to electric stimulation, as a result of the Maxwell stress. EAPs have found broad applications ranging from soft robots to implanted medical devices, energy harvesters, and electromechanical systems.[248–251] Stretchable electrodes based on CNTs,[71,252,253] AgNWs,[252] CuNWs,[109] and crumpled graphene[111] have been used to form EAP actuators. In EAP actuators, stretchable conductors are able to meet the mechanical and electrical requirements, i.e., they can withstand repeated large deformation with sufficient electrical conductance to distribute charges evenly and have little constraint on the EAP deformation.[254] An area strain of 100% was reported for VHB 4905 with CNT thin films sprayed on both sides[71] and 200% for VHB 4905 with CuNW films as the electrodes.[109] The transmittance of the EAP actuators can be tuned by the deformation, leading to actuators with tunable transmittance. The transmittance of CNT- and CuNW-based actuators increased as the area expanded, due to the decreased density of the CNTs[71] and CuNWs.[109] The widely tunable transmittance (from 13% to 58%, as shown in **Figure 16**a) of CuNW-based actuators means they can be used as light valves.[109] Moreover, for the actuators employing crumpled graphene as the electrodes, the unfolding of the crumpled structure (Figure 10f) during actuation (with 100% area strain) tuned the transmittance from ca. 40% to ca. 60% (Figure 16b and c).[111]

Pei's group introduced bistable electroactive polymers (BSEPs), for example, PtBA, as dielectric elastomers to form actuators that possess the bistable electrically-induced actuation imparted by temperature control across the glass transition.[68,249] The BSEPs used are rigid at room temperature, and become rubbery and thus deformable by the electric field above the glass-transition temperature. Upon cooling below the glass-transition temperature, the deformation and rigid shape can be locked even when the voltage is turned off, allowing for rigid-to-rigid bistable deformations, which can be useful in developing Braille displays.[249] The AgNW–PtBA composite modified by AA can be used as both Joule heating electrodes to supply the temperature above the glass-transition temperature and electrodes to apply a high voltage for actuation. As indicated in Figure 16d, the low voltage (V_L) for Joule heating (heating rate as high as 17 °C s^{-1}) was applied horizontally across the AgNW composites, and the high voltage (V_H) for actuation was applied to the top electrode. Repeatable out-of-plane actuation up to 68% was obtained at 45 MV m^{-1} (Figure 16e).[249] In addition to the electrostatic actuation only, the compliant electrodes could allow for smart actuation with resistive or capacitive sensing of the strain during the actuation.[254]

7.5. Stretchable Energy-Storage Devices

Stretchable energy-storage and conversion devices that can accommodate large strains represent another indispensable part of stretchable electronics. Interested readers are referred to recent reviews on this topic including stretchable supercapacitors, batteries, and solar cells.[13,255,256] Here, we focus on stretchable energy-storage devices based on nanomaterial-enabled stretchable conductors. As an important class of energy-storage devices, supercapacitors possess the advantages of high power density, fast charging/discharging, and long cycle life.[257,258] Typically, a supercapacitor is composed of three components: the electrode, the electrolyte, and the separator, where the electrical charges are stored on high-surface-area conducting materials.[257,259] Due to their high specific surface area, good electrolyte accessibility, good electrical properties, and excellent mechanical and thermal stabilities, CNTs and graphene have been widely investigated as potential candidates to replace traditional mesoporous carbon and activated carbon as electrodes.[202,257,258,260]

Recently CNT-based[38,101,261,262] and graphene-based[124,263] stretchable conductors were employed to fabricate stretchable supercapacitors. The power density (P) in a supercapacitor is determined by $P = V^2/4R_S$, where V is the voltage and R_S is the equivalent series resistance. Hence, constant R_S under stretching is required to maintain a constant power density in stretchable supercapacitors.[38] Yu et al. reported stretchable supercapacitors using electrodes based on a periodically buckled, sinusoidal SWNT macrofilm (2D network of randomly oriented SWNTs); the sinusoidal SWNT macrofilm was formed by transferring the macrofilm onto a prestrained PDMS (30%) followed by release of the prestrained PDMS.[38] The supercapacitors had stretchability up to 30% without much deterioration in capacitance, cycling stability, power, and energy density. Their more recent

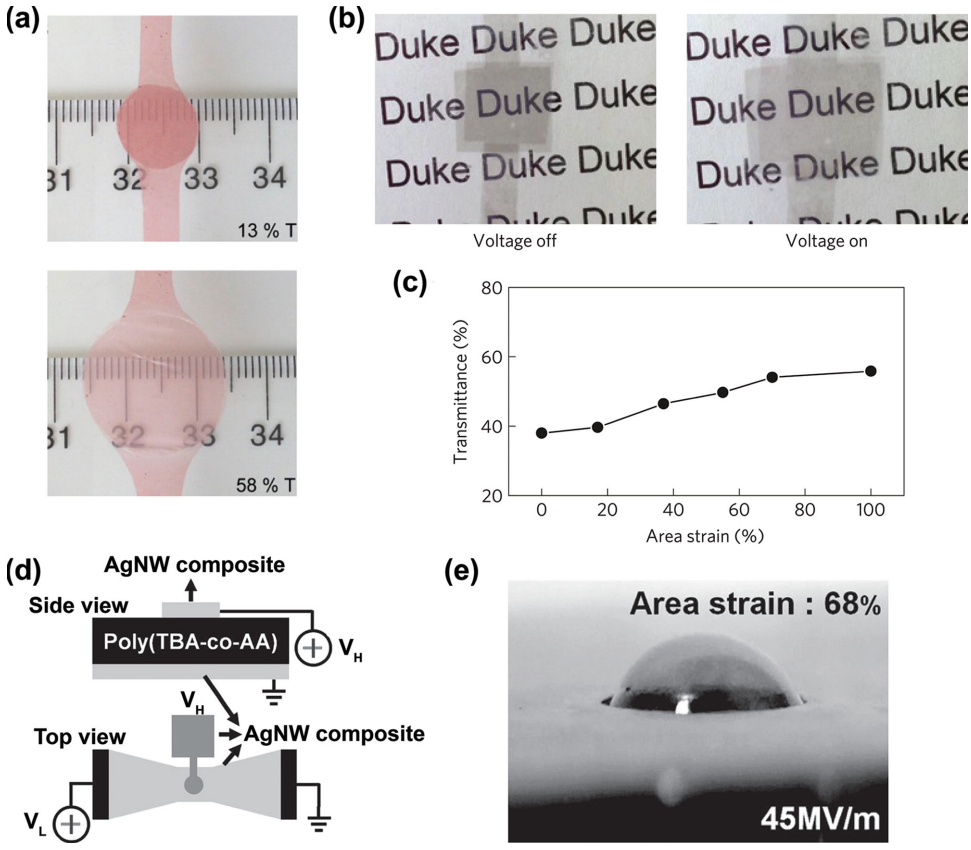

Figure 16. a) A CuNWs based actuator before and after actuation with a 4.8 kV voltage. Before actuation, the actuator shows transmittance of 13% (top). After actuated to an area strain of 200%, the transmittance increases to 58% (bottom). Reproduced with permission.[109] Copyright 2013, American Chemical Society. An actuator with crumpled graphene as electrodes: b) The area of actuators expanded with area strain over 100% as the voltage was applied. c) Transmittance of the actuator as a function of the area actuation strain. b,c) Reproduced with permission.[111] Copyright 2013, Nature Publishing Group. d) A schematic illustration of the BSEP actuator using AgNW polymer composite as both the Joule heating electrodes and compliant electrodes for applying high voltage. e) Photograph showing the deformed circular active area of BSEP actuator under electric field of 45 MV m^{-1}. d,e) Reproduced with permission.[68] Copyright 2012, John Wiley and Sons.

work[261] adopted an elastomeric electrospun PU separator into the supercapacitor (**Figure 17**a) and tested the performance of the stretchable supercapacitors under real-time dynamic situations. The stretchable supercapacitors showed stable performances under dynamic stretching/release with different strain rates, in addition to under a mechanically static state,[38] as shown in Figure 17b. The variation of the capacitive behavior was observed to be within 2% for all the strain rates. Using a similar prestrain–release–buckling strategy, Niu et al. employed SWNT films with a continuous reticulate architecture as electrodes, which were transferred onto a PDMS substrate with an enhanced prestrain level (100%) to generate the buckling structure.[101] Stretchable supercapacitors with a high stretchability up to 120% were achieved. The schematic of this type of supercapacitor is shown in Figure 17c. The superior stretchability was ascribed to the buckled patterns, as well as to the continuous 2D reticulate structure of the SWNT. A maximum power density of 32 kW kg^{-1} was obtained and it remained nearly constant up to 120% strain. As can be seen from Figure 17d, there is no obvious change in galvanostatic charge/discharge curves with or without strain. The specific capacitances were 48 F g^{-1} and 53 F g^{-1} for zero and 120% strain, respectively.

With wrinkled graphene electrodes grown on wrinkled copper films (Figure 10e), transparent supercapacitors that can be stretched to 40% strain without compromising much of the electrochemical behaviors (i.e., CVs, charge/discharge performance, and specific capacitance) were demonstrated.[124] Adopting the prestrain–release–buckling strategy, crumpled graphene papers (paper-like sheets fabricated from graphene oxide) with similar structures to those shown in Figure 10f were used to develop extremely stretchable supercapacitors.[263] To generate the crumpled structures, the graphene papers were attached to elastomeric substrates prestrained unequally (400% and 50%) or biaxially (400% and 400%) along two perpendicular directions and followed by releasing the strain sequentially. The resultant supercapacitors tested with aqueous H_2SO_4 solution can be stretched up to 300% uniaxial strain or 800% areal strain, with specific capacitance of 166–196 F g^{-1} at a discharge rate of 1 A g^{-1} and good stability over 1000 cycles of stretch/relax. An all solid state supercapacitor with polymer gel as the electrolyte and separator was further demonstrated, which maintained good performance under large deformations (150% uniaxial strain or 300% areal strain).

Employing AgNWs embedded into a PDMS matrix as both the stretchable electroactive material and current collector, zinc

DOI: 10.1002/adma.201404446

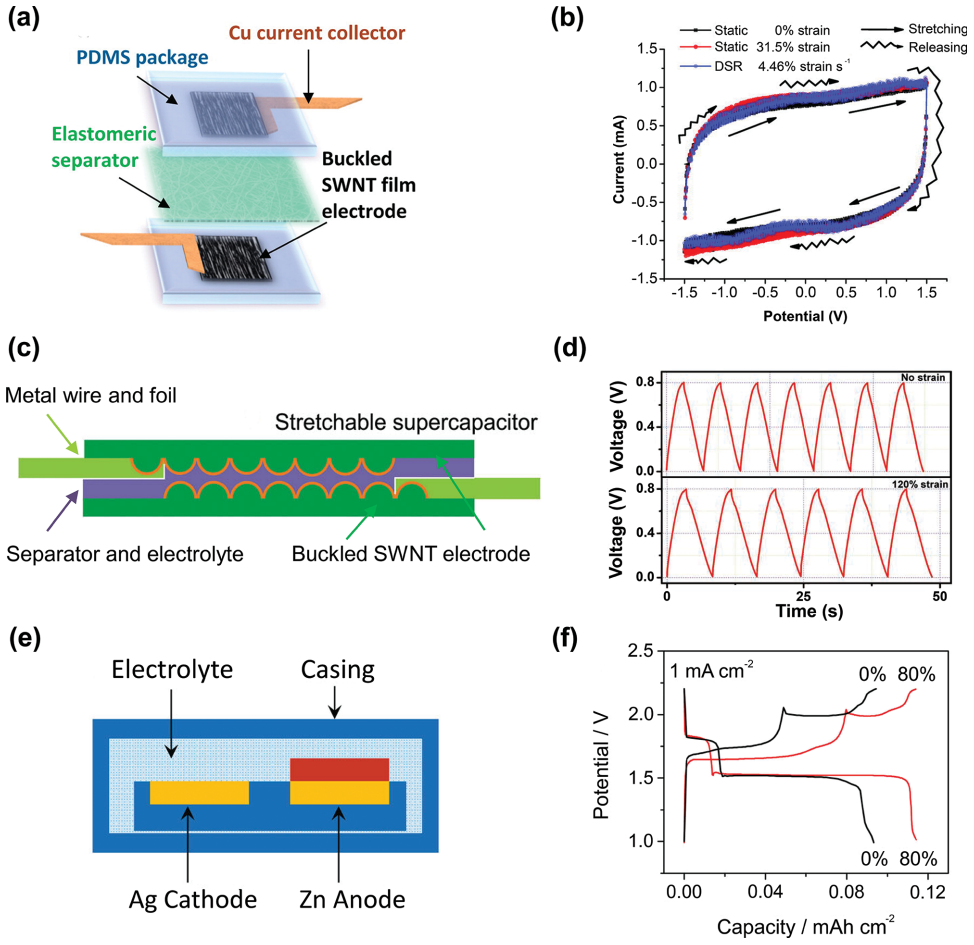

Figure 17. Dynamically stretchable supercapacitors based on buckled SWNT macrofilm: a) Schematic illustration of the stretchable supercapacitor. b) Cyclic voltammograms of the stretchable supercapacitors under the dynamic stretching/releasing mode at scan rates 4.46% strain s^{-1}. The curves shift between the two CV curves under statically applied minimum (0%) and maximum (31.5%) strain. a,b) Reproduced with permission.[261] Copyright 2012, American Chemical Society. Stretchable supercapacitors with buckled SWNT films having continuous reticulate architecture as electrodes: c) Schematic illustration of the supercapacitor. d) The galvanostatic charge/discharge curves for buckled SWNT film based stretchable supercapacitors with and without 120% strain. c,d) Reproduced with permission.[101] Copyright 2012, John Wiley and Sons. Stretchable Ag–Zn batteries with AgNW–PDMS electrodes: e) Schematic illustration of the stretchable battery. f) Charge/discharge curves for the battery without strain and with 80% strain. e,f) Reproduced with permission.[105] Copyright 2013, John Wiley and Sons.

(Zn) electroplated on a AgNW/PDMS substrate as the anode, Lee and co-workers[105] demonstrated stretchable Ag–Zn batteries, as illustrated in Figure 17e. The two electrodes and the liquid electrolyte were encapsulated in a PDMS casing. The charge/discharge curves for the battery without strain and with 80% strain are shown in Figure 17f. The areal capacity of 0.11 mA h cm^{-2} was observed for the battery without strain The stretchable battery maintained its functionality in the highly stretched states, exhibiting an areal capacity of 0.09 mA h cm^{-2} under 80% tensile strain. Development of stretchable and highly efficient energy-storage devices will help achieve better energy economy and facilitate the realization of self-powered wearable electronics.

7.6. Other Applications

In addition to their applications like interconnects, LEDs, sensors, actuators, and energy-storage devices, stretchable conductors are being explored as other components in stretchable/wearable electronics. Motivated by the recent progress in the wearable electronics and the need for conformal wireless communication, a variety of flexible and stretchable antennas based on nanomaterial-enabled stretchable conductors have been developed, including conductive composite mat of AgNPs and rubber fibers,[112] vertically grown CNTs embedded in a polymer,[264] and AgNWs embedded in PDMS.[265,266] By using two AgNW–PDMS sheets as the radiating element and the ground plane with a dielectric layer sandwiched in between, our group[265] demonstrated a 3 GHz microstrip patch antenna and a 6 GHz 2-element patch array. The resonant frequency of the AgNW/PDMS patch antennas slightly increased with increasing tensile strain in the range of 0–15% (**Figure 18**a and b). The variability was small, such that most receivers were able to pick up the signal even if the antenna was stretched, but with a sensitive enough receiver, the antenna could actually function as a strain sensor in its own right. A wider range of stretchability

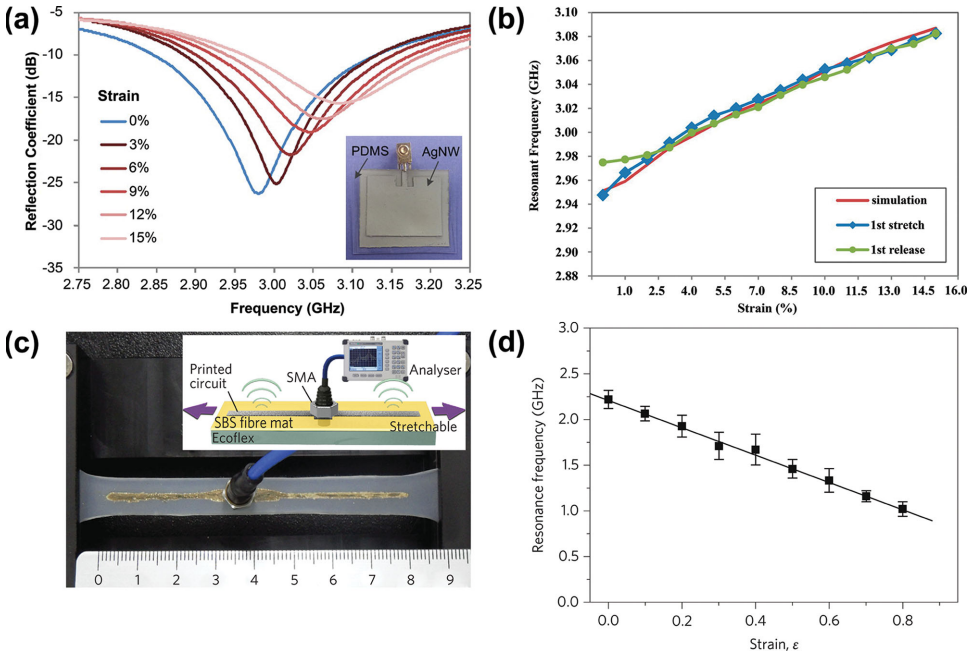

Figure 18. Stretchable microstrip patch antenna composed of AgNW–PDMS stretchable conductors: a) Frequency response of reflection coefficient for tensile strains ranging from 0% to 15%. The inset shows the photograph of the fabricated stretchable microstrip patch antenna. b) Simulation and measured resonant frequency during stretching and releasing under tensile strain from 0% to 15%. a,b) Reproduced with permission.[265] Copyright 2014, American Chemical Society. Half-wave dipole antenna based on electrospun Ag/SBS composite fiber mats fabricated by nozzle-printing: c) Photograph of the half-wave dipole antenna. The inset shows the schematic illustration of the structure. d) Resonance frequency of the dipole antenna as a function of tensile strain. c,d) Reproduced with permission.[112] Copyright 2012, Nature Publishing Group.

and tunability was demonstrated in dipole antennas based on Ag/SBS composite fiber mats (Figure 18c and d). A reliable and linear decrease of the resonance frequency was observed for tensile strains up to 80%, as shown in Figure 18d.[112] These pieces of work indicated a route in terms of materials and fabrication techniques to achieve other types of stretchable antennas with more-complex patterns and multilayer structures.

In another application, stretchable photodetectors comprising AgNW percolating networks as electrodes and ZnO NWs[267] (**Figure 19**a) or Zn_2SnO_4 NWs[120] (Figure 19b) as the channel were developed. The whole structures were fully embedded into PDMS to improve the stretchability. For the ZnO-NW-based photodetector, the device functioned well under a large strain of 100% and showed great stability against adhesive testing and cyclic stretching under 80% strain. For the Zn_2SnO_4-NW-based one, a transparent and stretchable photodetector was realized with response time of ca. 0.8 s and reset time of ca. 3 s. The functionalities were maintained for stretching with up to 50% strain. Stretchable electrochromic devices with AgNW–PDMS elastic conductors and a WO_3 active layer are shown in Figure 19c and d.[268] A coloration time of 4 s and a bleaching time of 25 s for the relaxed state and a coloration time of 9 s and a bleaching time of 43 s for the stretched state (50% strain) were observed. These stretchable electrochromic devices were further implanted onto a cotton textile substrate and showed good mechanical robustness and proper functions under deformation.

The feasibility of applying stretchable conductors in transistors has also been demonstrated.[36,125,115] With a higher electrical breakdown voltage, as compared with AgNW or graphene electrodes, graphene–AgNW hybrid structures were applied as source/drain electrodes in In–Ga–Zn–O (IGZO) thin-film transistors (Figure 19e), which exhibited high transparency and flexibility.[125] A mobility of 8.2 $cm^2\ V^{-1}\ s^{-1}$ and an on/off ratio of ca. 10^6 were achieved. As shown in Figure 19f, with Au nanosheets[269] as the source/drain and gate electrodes, a polyelectrolyte gel as the gate dielectric, electrospun poly(3-hexylthiophene) (P3HT) nanofibers as the channel material, and an electrospun SBS nanofiber mat as the stretchable substrate, a highly stretchable transistor was fabricated by Jeong and co-workers[115] Au nanosheets on stretchable SBS nanofibers showed enhanced electrostability. A constant resistance was achieved for strains up to 90%. A stable mobility of ca. 18 $cm^2\ V^{-1}\ s^{-1}$ and an on/off ratio of ca. 10^5 were observed for 1500 cycles of stretching under a tensile strain of 70%.

The advantages of stretchable conductors over flat and rigid ones have also been demonstrated for bioelectronic sensing. CNTs and AgNWs have been used in dry bioelectrodes for electrophysiology measurements, such as electrocardiograms (ECGs), electroencephalograms (EEGs), and electromyograms (EMGs)[270–272] to overcome the limitations of the widely used pre-gelled silver/silver chloride (Ag/AgCl) wet electrodes. The gel can cause skin irritation and dries over time. Also, the conductivity of the gel is sensitive to sweat, which usually results in signal degradation.[270,272,273] The dry electrodes, in contrast, can avoid any skin irritation.[270,274] CNT-based dry electrodes, as an example, have been shown to be robust against sweat.[272] One challenge for dry electrodes, as well as wet electrodes is to mitigate motion artifacts. Stretchable and compliant dry

Adv. Mater. **2015**,
DOI: 10.1002/adma.201404446

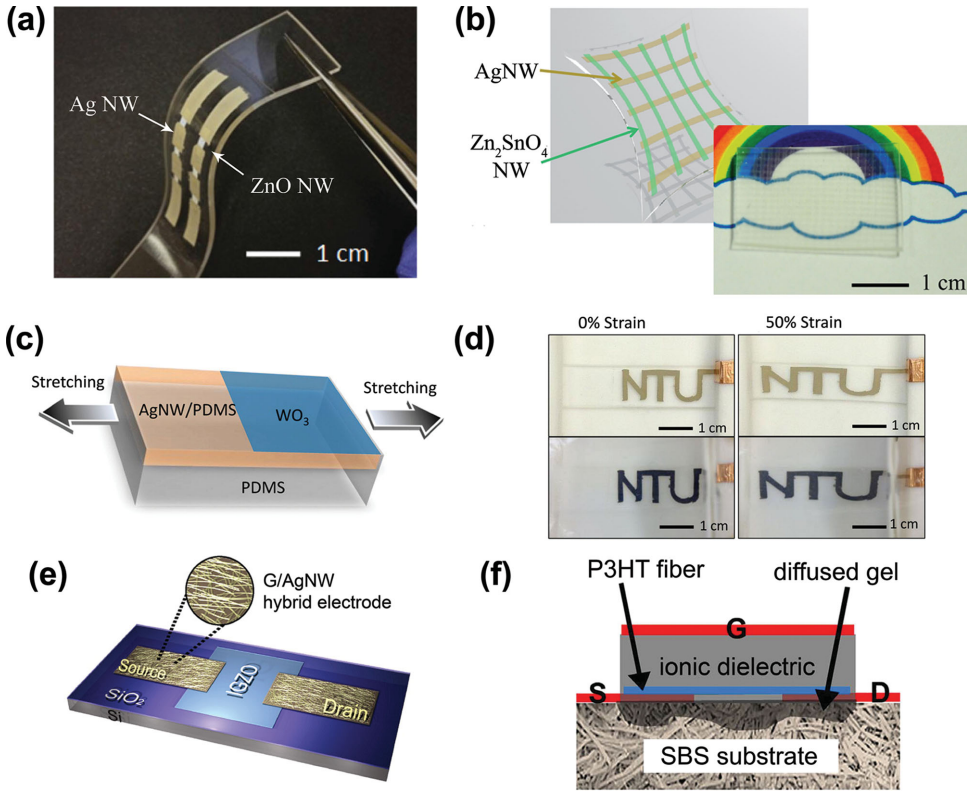

Figure 19. Stretchable photodetectors using AgNW network as electrodes: a) Photograph of the stretchable photodetectors using ZnO NW as the channel. Three photodetectors are connected in series. Reproduced with permission.[267] Copyright 2013, John Wiley and Sons. b) Schematic illustration (left) and photograph (right) of transparent and stretchable photodetectors with Zn_2SnO_4 NW as the channel. Reproduced with permission.[120] Copyright 2014, Royal Society of Chemistry. Stretchable and wearable electrochromatic devices using stretchable AgNW–PDMS conductors: c) Schematic of the electrochromatic device. d) Relaxed (left) and stretched (with 50% strain) (right) conditions for the electrochromatic device in bleached (top) and colored (bottom) states. c,d) Reproduced with permission.[268] Copyright 2014, American Chemical Society. e) Schematic of oxide semiconductor transistors with graphene/AgNW hybrid electrodes. Reproduced with permission.[125] Copyright 2013, American Chemical Society. f) Schematic of the stretchable transistors with Au nanosheets as S/D electrodes and gate electrode. Reproduced with permission.[115] Copyright 2014, John Wiley and Sons.

electrodes, made of CNTs dispersed in PDMS, were found to achieve better contact during motion, and thus reduced motion artifacts.[272] AgNW-based dry electrodes have been recently demonstrated to achieve excellent signal quality (comparable with that of Ag/AgCl wet electrodes) and fewer motion artifacts than with the wet electrodes.[275] The high signal fidelity under static, motion, and sweating conditions in conjunction with their non-irritating and biocompatible nature makes CNT-based stretchable dry electrodes suitable for long-term health monitoring.

In view of the exciting progress and the ongoing efforts on individual stretchable components (e.g., interconnects, sensors, actuators, supercapacitors, antennas, and transistors), it is reasonable to foresee the emergence of whole stretchable and wearable systems that combine these stretchable-conductor-based devices and other necessary circuit components in the next few years.

8. Concluding Remarks and Perspective

Connectors and electrodes that can sustain large strain are indispensable components of stretchable electronics. By harnessing the electric conductivity of nanomaterials and the stretchability of elastomers via plentiful types of stretchable structures, nanomaterial-enabled stretchable conductors that possess high electric conductivity and possibly high optical transparency have been realized. For example, conductivity higher than 5000 S cm^{-1} (opaque conductors),[41,60] transmittance larger than 90% with resistance less than 100 Ω sq^{-1},[62,69,73,125] and stretchability of ca. 500%[62,79,111] have been demonstrated. While most conductors are stretchable in one direction, some have already been demonstrated to be biaxially stretchable.[39,119,121]

Notwithstanding the outstanding performances of nanomaterial-enabled stretchable conductors, further development is needed in several directions, including nanomaterial synthesis, processing (manufacturing), and heterogeneous integration. Complementary to the technological advances, the underlying science encompasses many research topics of fundamental interest, from micro-/nanomechanics, to charge transport and its coupling to strain, to adhesion and interface science. As the building blocks of stretchable conductors, the advancements in large-scale, low-cost synthesis of high-quality nanomaterials will greatly facilitate the development of stretchable conductors. To further improve the conductivity, continuing efforts should be devoted to the effective doping of CNTs and graphene, and to the reduction of junction resistance in metallic NW networks. Percolation theory predicts that longer NWs lead to conductors

with a better balance of conductivity and transmittance. Haze is a problem for NWs with large diameters.[127,176] However, the synthesis of long and thin NWs with uniform diameter and good quality is still challenging.[76,87]

Scalable, high-rate nanomanufacture of stretchable conductors based on nanomaterials is critically needed. The top-down approach has seen remarkable success for stretchable electronics due to its compatibility with batch fabrication.[19] While it is challenging for bottom-up assembly/patterning of nanomaterials[276] to achieve the same level of precision, uniformity, and scalability, it is becoming feasible when combined with existing printing methods. Recent progress in screen-printing,[277,278] spray-coating,[39,175,176,279] ink-jet printing,[280–284] aerosol jet printing,[285–287] and gravure printing[288,289] of a variety of nanomaterials has been promising. Moreover, such printing methods typically offer a much lower cost than top-down micro/nano-fabrication.

Heterogeneous integration of nanomaterial-enabled stretchable conductors into stretchable systems represents another critical need. Key issues include interface bonding between the nanomaterials and substrates under large deformation, as well as the large contact resistance between the nanomaterial-based electrodes and other device components.[128] Mechanics has been playing an essential role in the development of thin-film-based stretchable electronics;[57,157,290] it is equally so for nanomaterial-based stretchable electronics. It is known that, individually, nanomaterials exhibit superior mechanical properties compared with their thin-film counterparts. Hence mechanics at the interface of nanomaterials and polymer substrates is of particular importance, e.g., considering the magnitude difference of about five orders in their Young's moduli. Study into the interface mechanics between nanomaterials and polymer substrates in the context of stretchable electronics is emer ging.[33,34,58,291,292]

Nanoscale science and engineering has been one of the most active research fields for more than two decades. Our understanding of nanoscale phenomena, materials, and devices has progressed to the point where we can make substantial strides in nanomaterial-enabled applications. As highlighted in this review, impressive advancements have been made to nanomaterial-enabled stretchable conductors over the past five years or so. The related stretchable devices will significantly expand to many areas where electronics are used. Some of the most compelling areas, in our view, are in the healthcare sector. Wearable healthcare, a paradigm shift in health informatics that monitors individual health conditions, is rapidly emerging. Novel nanomaterials with superior properties, innovative assembly/patterning methods, and new concepts for structural design, as well as inspiration from stretchable electronics using top-down fabricated structures[9] will accelerate the advance of this emerging field with broad applications in wearable sensors for health and activity monitoring, novel artificial skins for robots and prosthetics, conformal and intelligent interfaces, such as used in aircraft and smart homes, to name just a few.

Acknowledgements

This material is based on work supported by the National Science Foundation (NSF) through the ASSIST Engineering Research Center at NC State (EEC-1160483). Y.Z. would like to additionally acknowledge the NSF (EFRI-1240438) for support.

Received: September 26, 2014
Revised: November 24, 2014
Published online:

[1] M. L. Hammock, A. Chortos, B. C.-K. Tee, J. B. -H. Tok, Z. Bao, *Adv. Mater.* **2013**, *25*, 5997.
[2] S. R. Forrest, *Nature* **2004**, *428*, 911.
[3] X. Duan, C. Niu, V. Sahi, J. Chen, J. W. Parce, S. Empedocles, J. L. Goldman, *Nature* **2003**, *425*, 274.
[4] K. Takei, T. Takahashi, J. C. Ho, H. Ko, A. G. Gillies, P. W. Leu, R. S. Fearing, A. Javey, *Nat. Mater.* **2010**, *9*, 821.
[5] S. Xu, Y. Qin, C. Xu, Y. Wei, R. Yang, Z. L. Wang, *Nat. Nanotechnol.* **2010**, *5*, 366.
[6] S. Ju, A. Facchetti, Y. Xuan, J. Liu, F. Ishikawa, P. Ye, C. Zhou, T. J. Marks, D. B. Janes, *Nat. Nanotechnol.* **2007**, *2*, 378.
[7] M. C. McAlpine, H. Ahmad, D. Wang, J. R. Heath, *Nat. Mater.* **2007**, *6*, 379.
[8] M. C. McAlpine, R. S. Friedman, C. M. Lieber, *Proc. IEEE* **2005**, *93*, 1357.
[9] J. A. Rogers, T. Someya, Y. Huang, *Science* **2010**, *327*, 1603.
[10] Z. Suo, *MRS Bull.* **2012**, *37*, 218.
[11] S. Wagner, S. Bauer, *MRS Bull.* **2012**, *37*, 207.
[12] T. Sekitani, T. Someya, *Adv. Mater.* **2010**, *22*, 2228.
[13] D. J. Lipomi, Z. Bao, *Energy Environ. Sci.* **2011**, *4*, 3314.
[14] J.-H. Ahn, J. H. Je, *J. Phys. D: Appl. Phys.* **2012**, *45*, 103001.
[15] D.-H. Kim, J.-H. Ahn, W. M. Choi, H.-S. Kim, T.-H. Kim, J. Song, Y. Y. Huang, Z. Liu, C. Lu, J. A. Rogers, *Science* **2008**, *320*, 507.
[16] D.-H. Kim, J. Song, W. M. Choi, H.-S. Kim, R.-H. Kim, Z. Liu, Y. Y. Huang, K.-C. Hwang, Y.-W. Zhang, J. A. Rogers, *Proc. Natl. Acad. Sci. USA* **2008**, *105*, 18675.
[17] W. M. Choi, J. Song, D.-Y. Khang, H. Jiang, Y. Y. Huang, J. A. Rogers, *Nano Lett.* **2007**, *7*, 1655.
[18] S.-I. Park, Y. Xiong, R.-H. Kim, P. Elvikis, M. Meitl, D.-H. Kim, J. Wu, J. Yoon, C.-J. Yu, Z. Liu, Y. Huang, K.-C. Hwang, P. Ferreira, X. Li, K. Choquette, J. A. Rogers, *Science* **2009**, *325*, 977.
[19] D. H. Kim, J. Xiao, J. Song, Y. Huang, J. A. Rogers, *Adv. Mater.* **2010**, *22*, 2108.
[20] M. Gonzalez, F. Axisa, M. V. Bulcke, D. Brosteaux, B. Vandevelde, J. Vanfleteren, *Microelectron. Reliab.* **2008**, *48*, 825.
[21] D. Brosteaux, F. Axisa, M. Gonzalez, J. Vanfleteren, *IEEE Electron Device Lett.* **2007**, *28*, 552.
[22] H. C. Ko, M. P. Stoykovich, J. Song, V. Malyarchuk, W. M. Choi, C.-J. Yu, J. B. Geddes Iii, J. Xiao, S. Wang, Y. Huang, J. A. Rogers, *Nature* **2008**, *454*, 748.
[23] D.-H. Kim, N. Lu, R. Ma, Y.-S. Kim, R.-H. Kim, S. Wang, J. Wu, S. M. Won, H. Tao, A. Islam, K. J. Yu, T.-i. Kim, R. Chowdhury, M. Ying, L. Xu, M. Li, H.-J. Chung, H. Keum, M. McCormick, P. Liu, Y.-W. Zhang, F. G. Omenetto, Y. Huang, T. Coleman, J. A. Rogers, *Science* **2011**, *333*, 838.
[24] D. Son, J. Lee, S. Qiao, R. Ghaffari, J. Kim, J. E. Lee, C. Song, S. J. Kim, D. J. Lee, S. W. Jun, S. Yang, M. Park, J. Shin, K. Do, M. Lee, K. Kang, C. S. Hwang, N. Lu, T. Hyeon, D.-H. Kim, *Nat. Nanotechnol.* **2014**, *9*, 397.
[25] D.-H. Kim, N. Lu, R. Ghaffari, Y.-S. Kim, S. P. Lee, L. Xu, J. Wu, R.-H. Kim, J. Song, Z. Liu, J. Viventi, B. d. Graff, B. Elolampi, M. Mansour, M. J. Slepian, S. Hwang, J. D. Moss, S.-M. Won, Y. Huang, B. Litt, J. A. Rogers, *Nat. Mater.* **2011**, *10*, 316.
[26] D.-H. Kim, R. Ghaffari, N. Lu, J. A. Rogers, *Annu. Rev. Biomed. Eng.* **2012**, *14*, 113.

[27] B. Wu, A. Heidelberg, J. J. Boland, *Nat. Mater.* **2005**, *4*, 525.
[28] T. Zhu, J. Li, *Prog. Mater Sci.* **2010**, *55*, 710.
[29] G. Richter, K. Hillerich, D. S. Gianola, R. Monig, O. Kraft, C. A. Volkert, *Nano Lett.* **2009**, *9*, 3048.
[30] Y. Zhu, F. Xu, Q. Qin, W. Y. Fung, W. Lu, *Nano Lett.* **2009**, *9*, 3934.
[31] F. Xu, Q. Qin, A. Mishra, Y. Gu, Y. Zhu, *Nano Res.* **2010**, *3*, 271.
[32] Y. Zhu, Q. Qin, F. Xu, F. Fan, Y. Ding, T. Zhang, B. J. Wiley, Z. L. Wang, *Phys. Rev. B* **2012**, *85*, 045443.
[33] F. Xu, W. Lu, Y. Zhu, *ACS Nano* **2010**, *5*, 672.
[34] S. Y. Ryu, J. Xiao, W. I. Park, K. S. Son, Y. Y. Huang, U. Paik, J. A. Rogers, *Nano Lett.* **2009**, *9*, 3214.
[35] F. Xu, M.-Y. Wu, N. S. Safron, S. S. Roy, R. M. Jacobberger, D. J. Bindl, J.-H. Seo, T.-H. Chang, Z. Ma, M. S. Arnold, *Nano Lett.* **2014**, *14*, 682.
[36] S.-K. Lee, B. J. Kim, H. Jang, S. C. Yoon, C. Lee, B. H. Hong, J. A. Rogers, J. H. Cho, J.-H. Ahn, *Nano Lett.* **2011**, *11*, 4642.
[37] L. Cai, J. Li, P. Luan, H. Dong, D. Zhao, Q. Zhang, X. Zhang, M. Tu, Q. Zeng, W. Zhou, S. Xie, *Adv. Funct. Mater.* **2012**, *22*, 5238.
[38] C. Yu, C. Masarapu, J. Rong, B. Wei, H. Jiang, *Adv. Mater.* **2009**, *21*, 4793.
[39] D. J. Lipomi, M. Vosgueritchian, B. C. Tee, S. L. Hellstrom, J. A. Lee, C. H. Fox, Z. Bao, *Nat. Nanotechnol.* **2011**, *6*, 788.
[40] T. Akter, W. S. Kim, *ACS Appl. Mater. Interfaces* **2012**, *4*, 1855.
[41] K.-Y. Chun, Y. Oh, J. Rho, J.-H. Ahn, Y.-J. Kim, H. R. Choi, S. Baik, *Nat. Nanotechnol.* **2010**, *5*, 853.
[42] Y. Shang, Y. Li, X. He, L. Zhang, Z. Li, P. Li, E. Shi, S. Wu, A. Cao, *Nanoscale* **2013**, *5*, 2403.
[43] M. K. Shin, J. Oh, M. Lima, M. E. Kozlov, S. J. Kim, R. H. Baughman, *Adv. Mater.* **2010**, *22*, 2663.
[44] T. A. Kim, H. S. Kim, S. S. Lee, M. Park, *Carbon* **2012**, *50*, 444.
[45] Y. Y. Huang, E. M. Terentjev, *Adv. Funct. Mater.* **2010**, *20*, 4062.
[46] Z. Spitalsky, D. Tasis, K. Papagelis, C. Galiotis, *Prog. Polym. Sci.* **2010**, *35*, 357.
[47] T. Sekitani, H. Nakajima, H. Maeda, T. Fukushima, T. Aida, K. Hata, T. Someya, *Nat. Mater.* **2009**, *8*, 494.
[48] G.-X. Chen, Y. Li, H. Shimizu, *Carbon* **2007**, *45*, 2334.
[49] Y. Huang, S. Ahir, E. Terentjev, *Phys. Rev. B* **2006**, *73*, 125422.
[50] T. Sekitani, Y. Noguchi, K. Hata, T. Fukushima, T. Aida, T. Someya, *Science* **2008**, *321*, 1468.
[51] B. K. Price, J. L. Hudson, J. M. Tour, *J. Am. Chem. Soc.* **2005**, *127*, 14867.
[52] M. Park, J. Park, U. Jeong, *Nano Today* **2014**, *9*, 244.
[53] F. Xu, X. Wang, Y. Zhu, Y. Zhu, *Adv. Funct. Mater.* **2012**, *22*, 1279.
[54] Y. Zhu, F. Xu, *Adv. Mater.* **2012**, *24*, 1073.
[55] K. Liu, Y. Sun, P. Liu, X. Lin, S. Fan, K. Jiang, *Adv. Funct. Mater.* **2011**, *21*, 2721.
[56] H.-W. Liang, Q.-F. Guan, L.-T. S. Zhu-Zhu, H.-B. Yao, X. Lei, S.-H. Yu, *Npg Asia Mater.* **2012**, *4*, e19.
[57] N. Bowden, S. Brittain, A. G. Evans, J. W. Hutchinson, G. M. Whitesides, *Nature* **1998**, *393*, 146.
[58] Q. Qin, Y. Zhu, *ACS Nano* **2011**, *5*, 7404.
[59] E. C. Garnett, W. Cai, J. J. Cha, F. Mahmood, S. T. Connor, M. G. Christoforo, Y. Cui, M. D. McGehee, M. L. Brongersma, *Nat. Mater.* **2012**, *11*, 241.
[60] F. Xu, Y. Zhu, *Adv. Mater.* **2012**, *24*, 5117.
[61] J. W. Durham III, Y. Zhu, *ACS Appl. Mater. Interfaces* **2012**, *5*, 256.
[62] P. Lee, J. Lee, H. Lee, J. Yeo, S. Hong, K. H. Nam, D. Lee, S. S. Lee, S. H. Ko, *Adv. Mater.* **2012**, *24*, 3326.
[63] S. Han, S. Hong, J. Ham, J. Yeo, J. Lee, B. Kang, P. Lee, J. Kwon, S. S. Lee, M. Y. Yang, S. H. Ko, *Adv. Mater.* **2014**, *26*, 5808.
[64] W. Ma, L. Song, R. Yang, T. Zhang, Y. Zhao, L. Sun, Y. Ren, D. Liu, L. Liu, J. Shen, Z. Zhang, Y. Xiang, W. Zhou, S. Xie, *Nano Lett.* **2007**, *7*, 2307.
[65] Z. Chen, W. Ren, L. Gao, B. Liu, S. Pei, H.-M. Cheng, *Nat. Mater.* **2011**, *10*, 424.
[66] Y. Shang, X. He, Y. Li, L. Zhang, Z. Li, C. Ji, E. Shi, P. Li, K. Zhu, Q. Peng, C. Wang, X. Zhang, R. Wang, J. Wei, K. Wang, H. Zhu, D. Wu, A. Cao, *Adv. Mater.* **2012**, *24*, 2896.
[67] Z. Yu, X. Niu, Z. Liu, Q. Pei, *Adv. Mater.* **2011**, *23*, 3989.
[68] S. Yun, X. Niu, Z. Yu, W. Hu, P. Brochu, Q. Pei, *Adv. Mater.* **2012**, *24*, 1321.
[69] W. Hu, X. Niu, L. Li, S. Yun, Z. Yu, Q. Pei, *Nanotechnology* **2012**, *23*, 344002.
[70] W. Hu, R. Wang, Y. Lu, Q. Pei, *J. Mater. Chem. C* **2014**, *2*, 1298.
[71] L. Hu, W. Yuan, P. Brochu, G. Gruner, Q. Pei, *Appl. Phys. Lett.* **2009**, *94*, 161108.
[72] H. Wu, L. Hu, M. W. Rowell, D. Kong, J. J. Cha, J. R. McDonough, J. Zhu, Y. Yang, M. D. McGehee, Y. Cui, *Nano Lett.* **2010**, *10*, 4242.
[73] J. Liang, L. Li, K. Tong, Z. Ren, W. Hu, X. Niu, Y. Chen, Q. Pei, *ACS Nano* **2014**, *8*, 1590.
[74] T. Tokuno, M. Nogi, M. Karakawa, J. Jiu, T. T. Nge, Y. Aso, K. Suganuma, *Nano Res.* **2011**, *4*, 1215.
[75] L. Yang, T. Zhang, H. Zhou, S. C. Price, B. J. Wiley, W. You, *ACS Appl. Mater. Interfaces* **2011**, *3*, 4075.
[76] J. Lee, P. Lee, H. Lee, D. Lee, S. S. Lee, S. H. Ko, *Nanoscale* **2012**, *4*, 6408.
[77] A. R. Madaria, A. Kumar, F. N. Ishikawa, C. Zhou, *Nano Res.* **2010**, *3*, 564.
[78] H. Guo, N. Lin, Y. Chen, Z. Wang, Q. Xie, T. Zheng, N. Gao, S. Li, J. Kang, D. Cai, D.-L. Peng, *Sci. Rep.* **2013**, *3*, 2323.
[79] J. Y. Woo, K. K. Kim, J. Lee, J. T. Kim, C.-S. Han, *Nanotechnology* **2014**, *25*, 285203.
[80] J. Lee, P. Lee, H. B. Lee, S. Hong, I. Lee, J. Yeo, S. S. Lee, T. S. Kim, D. Lee, S. H. Ko, *Adv. Funct. Mater.* **2013**, *23*, 4171.
[81] I. K. Moon, J. I. Kim, H. Lee, K. Hur, W. C. Kim, H. Lee, *Sci. Rep.* **2013**, *3*, 1112.
[82] J. L. Blackburn, T. M. Barnes, M. C. Beard, Y.-H. Kim, R. C. Tenent, T. J. McDonald, B. To, T. J. Coutts, M. J. Heben, *ACS Nano* **2008**, *2*, 1266.
[83] Z. Xu, Z. Liu, H. Sun, C. Gao, *Adv. Mater.* **2013**, *25*, 3249.
[84] A. Kasry, M. A. Kuroda, G. J. Martyna, G. S. Tulevski, A. A. Bol, *ACS Nano* **2010**, *4*, 3839.
[85] G. Pike, C. Seager, *Phys. Rev. B* **1974**, *10*, 1421.
[86] S. Kirkpatrick, *Rev. Mod. Phys.* **1973**, *45*, 574.
[87] D. Zhang, R. Wang, M. Wen, D. Weng, X. Cui, J. Sun, H. Li, Y. Lu, *J. Am. Chem. Soc.* **2012**, *134*, 14283.
[88] S. De, J. N. Coleman, *MRS Bull.* **2011**, *36*, 774.
[89] T. M. Barnes, M. O. Reese, J. D. Bergeson, B. A. Larsen, J. L. Blackburn, M. C. Beard, J. Bult, J. van de Lagemaat, *Adv. Energy Mater.* **2012**, *2*, 353.
[90] K. Ellmer, *Nat. Photonics* **2012**, *6*, 809.
[91] Q. Cao, J. A. Rogers, *Adv. Mater.* **2009**, *21*, 29.
[92] R. H. Baughman, A. A. Zakhidov, W. A. de Heer, *Science* **2002**, *297*, 787.
[93] H. Dai, *Acc. Chem. Res.* **2002**, *35*, 1035.
[94] M. Treacy, T. Ebbesen, J. Gibson, *Nature* **1996**, *381*, 678.
[95] M.-F. Yu, B. S. Files, S. Arepalli, R. S. Ruoff, *Phys. Rev. Lett.* **2000**, *84*, 5552.
[96] B. Peng, M. Locascio, P. Zapol, S. Li, S. L. Mielke, G. C. Schatz, H. D. Espinosa, *Nat. Nanotechnol.* **2008**, *3*, 626.
[97] E. T. Thostenson, Z. Ren, T.-W. Chou, *Compos. Sci. Technol.* **2001**, *61*, 1899.
[98] R. Graupner, J. Abraham, A. Vencelová, T. Seyller, F. Hennrich, M. M. Kappes, A. Hirsch, L. Ley, *Phys. Chem. Chem. Phys.* **2003**, *5*, 5472.
[99] J. W. Jo, J. W. Jung, J. U. Lee, W. H. Jo, *ACS Nano* **2010**, *4*, 5382.

[100] K. H. Kim, M. Vural, M. F. Islam, *Adv. Mater.* **2011**, *23*, 2865.
[101] Z. Niu, H. Dong, B. Zhu, J. Li, H. H. Hng, W. Zhou, X. Chen, S. Xie, *Adv. Mater.* **2012**, *25*, 1058.
[102] T. Kim, H. Song, J. Ha, S. Kim, D. Kim, S. Chung, J. Lee, Y. Hong, *Appl. Phys. Lett.* **2014**, *104*, 113103.
[103] U.-H. Shin, D.-W. Jeong, S.-H. Kim, H. W. Lee, J.-M. Kim, *ACS Appl. Mater. Interfaces* **2014**, *6*, 12909.
[104] M. Zu, Q. Li, G. Wang, J. H. Byun, T. W. Chou, *Adv. Funct. Mater.* **2012**, *23*, 789.
[105] C. Yan, X. Wang, M. Cui, J. Wang, W. Kang, C. Y. Foo, P. S. Lee, *Adv. Energy Mater.* **2014**, *4*, 1301396.
[106] P. Lee, J. Ham, J. Lee, S. Hong, S. Han, Y. D. Suh, S. E. Lee, J. Yeo, S. S. Lee, D. Lee, S. H. Ko, *Adv. Funct. Mater.* **2014**, *24*, 5671.
[107] J. Ge, H. B. Yao, X. Wang, Y. D. Ye, J. L. Wang, Z. Y. Wu, J. W. Liu, F. J. Fan, H. L. Gao, C. L. Zhang, S.-H. Yu, *Angew. Chem.* **2013**, *125*, 1698.
[108] H. L. Gao, L. Xu, F. Long, Z. Pan, Y. X. Du, Y. Lu, J. Ge, S. H. Yu, *Angew. Chem. Int. Ed.* **2014**, *53*, 4561.
[109] B. J. Wiley, J. Zang, A. Rathmell, J. Wu, X. Zhao, *Nano Lett.* **2013**, *13*, 2381.
[110] Y. Tang, S. Gong, Y. Chen, L. W. Yap, W. Cheng, *ACS Nano* **2014**, *8*, 5707.
[111] J. Zang, S. Ryu, N. Pugno, Q. Wang, Q. Tu, M. J. Buehler, X. Zhao, *Nat. Mater.* **2013**, *12*, 321.
[112] M. Park, J. Im, M. Shin, Y. Min, J. Park, H. Cho, S. Park, M.-B. Shim, S. Jeon, D.-Y. Chung, J. Bae, J. Park, U. Jeong, K. Kim, *Nat. Nanotechnol.* **2012**, *7*, 803.
[113] S. Chung, J. Lee, H. Song, S. Kim, J. Jeong, Y. Hong, *Appl. Phys. Lett.* **2011**, *98*, 153110.
[114] Y. Kim, J. Zhu, B. Yeom, M. Di Prima, X. Su, J.-G. Kim, S. J. Yoo, C. Uher, N. A. Kotov, *Nature* **2013**, *500*, 59.
[115] M. Shin, J. H. Song, G. H. Lim, B. Lim, J. J. Park, U. Jeong, *Adv. Mater.* **2014**, *26*, 3706.
[116] Y. Zhang, C. J. Sheehan, J. Zhai, G. Zou, H. Luo, J. Xiong, Y. Zhu, Q. Jia, *Adv. Mater.* **2010**, *22*, 3027.
[117] T. A. Kim, S.-S. Lee, H. Kim, M. Park, *RSC Adv.* **2012**, *2*, 10717.
[118] W. Hu, X. Niu, R. Zhao, Q. Pei, *Appl. Phys. Lett.* **2013**, *102*, 083303.
[119] X. Ho, J. Nie Tey, W. Liu, C. Kweng Cheng, J. Wei, *J. Appl. Phys.* **2013**, *113*, 044311.
[120] J. Wang, C. Yan, W. Kang, P. S. Lee, *Nanoscale* **2014**, *6*, 10734.
[121] D. C. Hyun, M. Park, C. Park, B. Kim, Y. Xia, J. H. Hur, J. M. Kim, J. J. Park, U. Jeong, *Adv. Mater.* **2011**, *23*, 2946.
[122] Y. Cheng, S. Wang, R. Wang, J. Sun, L. Gao, *J. Mater. Chem. C* **2014**, *2*, 5309.
[123] K. S. Kim, Y. Zhao, H. Jang, S. Y. Lee, J. M. Kim, K. S. Kim, J.-H. Ahn, P. Kim, J.-Y. Choi, B. H. Hong, *Nature* **2009**, *457*, 706.
[124] T. Chen, Y. Xue, A. K. Roy, L. Dai, *ACS Nano* **2013**, *8*, 1039.
[125] M.-S. Lee, K. Lee, S.-Y. Kim, H. Lee, J. Park, K.-H. Choi, H.-K. Kim, D.-G. Kim, D.-Y. Lee, S. Nam, J.-U. Park, *Nano Lett.* **2013**, *13*, 2814.
[126] L. Hu, H. S. Kim, J.-Y. Lee, P. Peumans, Y. Cui, *ACS Nano* **2010**, *4*, 2955.
[127] D. S. Hecht, L. Hu, G. Irvin, *Adv. Mater.* **2011**, *23*, 1482.
[128] L. Hu, H. Wu, Y. Cui, *MRS Bull.* **2011**, *36*, 760.
[129] L. Xiao, Z. Chen, C. Feng, L. Liu, Z.-Q. Bai, Y. Wang, L. Qian, Y. Zhang, Q. Li, K. Jiang, S. Fan, *Nano Lett.* **2008**, *8*, 4539.
[130] L. Cai, L. Song, P. Luan, Q. Zhang, N. Zhang, Q. Gao, D. Zhao, X. Zhang, M. Tu, F. Yang, W. Zhou, Q. Fan, J. Luo, W. Zhou, P. M. Ajayan, S. Xie, *Sci. Rep.* **2013**, *3*, 3048.
[131] K. Jiang, J. Wang, Q. Li, L. Liu, C. Liu, S. Fan, *Adv. Mater.* **2011**, *23*, 1154.
[132] X. Zhang, K. Jiang, C. Feng, P. Liu, L. Zhang, J. Kong, T. Zhang, Q. Li, S. Fan, *Adv. Mater.* **2006**, *18*, 1505.
[133] K. Jiang, Q. Li, S. Fan, *Nature* **2002**, *419*, 801.
[134] M. Zhang, S. Fang, A. A. Zakhidov, S. B. Lee, A. E. Aliev, C. D. Williams, K. R. Atkinson, R. H. Baughman, *Science* **2005**, *309*, 1215.
[135] M. Zhang, K. R. Atkinson, R. H. Baughman, *Science* **2004**, *306*, 1358.
[136] K. Liu, Y. Sun, L. Chen, C. Feng, X. Feng, K. Jiang, Y. Zhao, S. Fan, *Nano Lett.* **2008**, *8*, 700.
[137] C. Feng, K. Liu, J. S. Wu, L. Liu, J. S. Cheng, Y. Zhang, Y. Sun, Q. Li, S. Fan, K. Jiang, *Adv. Funct. Mater.* **2010**, *20*, 885.
[138] K. Liu, Y. Sun, X. Lin, R. Zhou, J. Wang, S. Fan, K. Jiang, *ACS Nano* **2010**, *4*, 5827.
[139] K. Liu, Y. Sun, R. Zhou, H. Zhu, J. Wang, L. Liu, S. Fan, K. Jiang, *Nanotechnology* **2010**, *21*, 045708.
[140] P. Liu, L. Liu, Y. Wei, K. Liu, Z. Chen, K. Jiang, Q. Li, S. Fan, *Adv. Mater.* **2009**, *21*, 3563.
[141] Y. Sun, K. Liu, J. Miao, Z. Wang, B. Tian, L. Zhang, Q. Li, S. Fan, K. Jiang, *Nano Lett.* **2010**, *10*, 1747.
[142] L. Zhang, C. Feng, Z. Chen, L. Liu, K. Jiang, Q. Li, S. Fan, *Nano Lett.* **2008**, *8*, 2564.
[143] R. Zhou, C. Meng, F. Zhu, Q. Li, C. Liu, S. Fan, K. Jiang, *Nanotechnology* **2010**, *21*, 345701.
[144] H. X. Zhang, C. Feng, Y. C. Zhai, K. L. Jiang, Q. Q. Li, S. S. Fan, *Adv. Mater.* **2009**, *21*, 2299.
[145] Q. Li, X. Zhang, R. F. DePaula, L. Zheng, Y. Zhao, L. Stan, T. G. Holesinger, P. N. Arendt, D. E. Peterson, Y. T. Zhu, *Adv. Mater.* **2006**, *18*, 3160.
[146] Q. Li, Y. Li, X. Zhang, S. B. Chikkannanavar, Y. Zhao, A. M. Dangelewicz, L. Zheng, S. K. Doorn, Q. Jia, D. E. Peterson, P. N. Arendt, Y. T. Zhu, *Adv. Mater.* **2007**, *19*, 3358.
[147] L. M. Ericson, H. Fan, H. Peng, V. A. Davis, W. Zhou, J. Sulpizio, Y. Wang, R. Booker, J. Vavro, C. Guthy, A. N. G. Parra-Vasquez, M. J. Kim, S. Ramesh, R. K. Saini, C. Kittrell, G. Lavin, H. Schmidt, W. W. Adams, W. E. Billups, M. Pasquali, W.-F. Hwang, R. H. Hauge, J. E. Fischer, R. E. Smalley, *Science* **2004**, *305*, 1447.
[148] R. Haggenmueller, H. Gommans, A. Rinzler, J. E. Fischer, K. Winey, *Chem. Phys. Lett.* **2000**, *330*, 219.
[149] Y.-L. Li, I. A. Kinloch, A. H. Windle, *Science* **2004**, *304*, 276.
[150] K. Koziol, J. Vilatela, A. Moisala, M. Motta, P. Cunniff, M. Sennett, A. Windle, *Science* **2007**, *318*, 1892.
[151] H. Zhao, Y. Zhang, P. D. Bradford, Q. Zhou, Q. Jia, F.-G. Yuan, Y. Zhu, *Nanotechnology* **2010**, *21*, 305502.
[152] A. B. Dalton, S. Collins, E. Munoz, J. M. Razal, V. H. Ebron, J. P. Ferraris, J. N. Coleman, B. G. Kim, R. H. Baughman, *Nature* **2003**, *423*, 703.
[153] P. Miaudet, S. Badaire, M. Maugey, A. Derre, V. Pichot, P. Launois, P. Poulin, C. Zakri, *Nano Lett.* **2005**, *5*, 2212.
[154] J. Foroughi, G. M. Spinks, G. G. Wallace, J. Oh, M. E. Kozlov, S. Fang, T. Mirfakhrai, J. D. Madden, M. K. Shin, S. J. Kim, R. H. Baughman, *Science* **2011**, *334*, 494.
[155] J. J. Vilatela, J. A. Elliott, A. H. Windle, *ACS Nano* **2011**, *5*, 1921.
[156] D.-Y. Khang, J. Xiao, C. Kocabas, S. MacLaren, T. Banks, H. Jiang, Y. Y. Huang, J. A. Rogers, *Nano Lett.* **2008**, *8*, 124.
[157] D.-Y. Khang, H. Jiang, Y. Huang, J. A. Rogers, *Science* **2006**, *311*, 208.
[158] B. S. Shim, W. Chen, C. Doty, C. Xu, N. A. Kotov, *Nano Lett.* **2008**, *8*, 4151.
[159] M. Havel, K. Behler, G. Korneva, Y. Gogotsi, *Adv. Funct. Mater.* **2008**, *18*, 2322.
[160] B. OConnor, C. Haughn, K.-H. An, K. P. Pipe, M. Shtein, *Appl. Phys. Lett.* **2008**, *93*, 223304.
[161] D. Ghosh, L. Martinez, S. Giurgola, P. Vergani, V. Pruneri, *Opt. Lett.* **2009**, *34*, 325.
[162] P. B. Catrysse, S. Fan, *Nano Lett.* **2010**, *10*, 2944.

Adv. Mater. **2015**,
DOI: 10.1002/adma.201404446

[163] M.-G. Kang, H. J. Park, S. H. Ahn, T. Xu, L. Guo, *IEEE J. Sel. Top. Quantum Electron.* **2010**, *16*, 1807.
[164] C. Yang, H. Gu, W. Lin, M. M. Yuen, C. P. Wong, M. Xiong, B. Gao, *Adv. Mater.* **2011**, *23*, 3052.
[165] D. Langley, G. Giusti, C. Mayousse, C. Celle, D. Bellet, J.-P. Simonato, *Nanotechnology* **2013**, *24*, 452001.
[166] Y. Sun, B. Gates, B. Mayers, Y. Xia, *Nano Lett.* **2002**, *2*, 165.
[167] Y. Sun, Y. Xia, *Adv. Mater.* **2002**, *14*, 833.
[168] M. Hu, J. Gao, Y. Dong, S. Yang, R. K. Li, *RSC Adv.* **2012**, *2*, 2055.
[169] B. Wiley, Y. Sun, Y. Xia, *Acc. Chem. Res.* **2007**, *40*, 1067.
[170] H. Wei, H. Xu, *Nanophotonics* **2012**, *1*, 155.
[171] J. Mock, S. Oldenburg, D. Smith, D. Schultz, S. Schultz, *Nano Lett.* **2002**, *2*, 465.
[172] A. Tao, F. Kim, C. Hess, J. Goldberger, R. He, Y. Sun, Y. Xia, P. Yang, *Nano Lett.* **2003**, *3*, 1229.
[173] W. Wang, Q. Yang, F. Fan, H. Xu, Z. L. Wang, *Nano Lett.* **2011**, *11*, 1603.
[174] Z. Li, K. Bao, Y. Fang, Y. Huang, P. Nordlander, H. Xu, *Nano Lett.* **2010**, *10*, 1831.
[175] A. R. Madaria, A. Kumar, C. Zhou, *Nanotechnology* **2011**, *22*, 245201.
[176] V. Scardaci, R. Coull, P. E. Lyons, D. Rickard, J. N. Coleman, *Small* **2011**, *7*, 2621.
[177] J.-Y. Lee, S. T. Connor, Y. Cui, P. Peumans, *Nano Lett.* **2008**, *8*, 689.
[178] S. De, T. M. Higgins, P. E. Lyons, E. M. Doherty, P. N. Nirmalraj, W. J. Blau, J. J. Boland, J. N. Coleman, *ACS Nano* **2009**, *3*, 1767.
[179] D. S. Leem, A. Edwards, M. Faist, J. Nelson, D. D. Bradley, J. C. de Mello, *Adv. Mater.* **2011**, *23*, 4371.
[180] X. Y. Zeng, Q. K. Zhang, R. M. Yu, C. Z. Lu, *Adv. Mater.* **2010**, *22*, 4484.
[181] Z. Yu, Q. Zhang, L. Li, Q. Chen, X. Niu, J. Liu, Q. Pei, *Adv. Mater.* **2011**, *23*, 664.
[182] W. Gaynor, G. F. Burkhard, M. D. McGehee, P. Peumans, *Adv. Mater.* **2011**, *23*, 2905.
[183] A. R. Rathmell, S. M. Bergin, Y. L. Hua, Z. Y. Li, B. J. Wiley, *Adv. Mater.* **2010**, *22*, 3558.
[184] M. Mohl, P. Pusztai, A. Kukovecz, Z. Konya, J. Kukkola, K. Kordas, R. Vajtai, P. M. Ajayan, *Langmuir* **2010**, *26*, 16496.
[185] Y. Chang, M. L. Lye, H. C. Zeng, *Langmuir* **2005**, *21*, 3746.
[186] M. Bognitzki, M. Becker, M. Graeser, W. Massa, J. H. Wendorff, A. Schaper, D. Weber, A. Beyer, A. Gölzhäuser, A. Greiner, *Adv. Mater.* **2006**, *18*, 2384.
[187] T. Subbiah, G. Bhat, R. Tock, S. Parameswaran, S. Ramkumar, *J. Appl. Polym. Sci.* **2005**, *96*, 557.
[188] A. Greiner, J. H. Wendorff, *Angew. Chem. Int. Ed.* **2007**, *46*, 5670.
[189] D. Li, Y. Xia, *Adv. Mater.* **2004**, *16*, 1151.
[190] Z.-M. Huang, Y.-Z. Zhang, M. Kotaki, S. Ramakrishna, *Compos. Sci. Technol.* **2003**, *63*, 2223.
[191] P.-C. Hsu, H. Wu, T. J. Carney, M. T. McDowell, Y. Yang, E. C. Garnett, M. Li, L. Hu, Y. Cui, *ACS Nano* **2012**, *6*, 5150.
[192] A. R. Rathmell, M. Nguyen, M. Chi, B. J. Wiley, *Nano Lett.* **2012**, *12*, 3193.
[193] I. N. Kholmanov, S. H. Domingues, H. Chou, X. Wang, C. Tan, J.-Y. Kim, H. Li, R. Piner, A. J. Zarbin, R. S. Ruoff, *ACS Nano* **2013**, *7*, 1811.
[194] K. S. Novoselov, A. K. Geim, S. Morozov, D. Jiang, Y. Zhang, S. Dubonos, I. Grigorieva, A. Firsov, *Science* **2004**, *306*, 666.
[195] S. Pang, Y. Hernandez, X. Feng, K. Müllen, *Adv. Mater.* **2011**, *23*, 2779.
[196] Y. Zhu, S. Murali, W. Cai, X. Li, J. W. Suk, J. R. Potts, R. S. Ruoff, *Adv. Mater.* **2010**, *22*, 3906.
[197] F. Bonaccorso, Z. Sun, T. Hasan, A. Ferrari, *Nat. Photonics* **2010**, *4*, 611.
[198] X. Huang, Z. Zeng, Z. Fan, J. Liu, H. Zhang, *Adv. Mater.* **2012**, *24*, 5979.
[199] Y. Shao, J. Wang, H. Wu, J. Liu, I. A. Aksay, Y. Lin, *Electroanalysis* **2010**, *22*, 1027.
[200] J. R. Potts, D. R. Dreyer, C. W. Bielawski, R. S. Ruoff, *Polymer* **2011**, *52*, 5.
[201] W. Choi, I. Lahiri, R. Seelaboyina, Y. S. Kang, *Crit. Rev. Solid State Mater. Sci.* **2010**, *35*, 52.
[202] J. Zhu, D. Yang, Z. Yin, Q. Yan, H. Zhang, *Small* **2014**, *10*, 3480.
[203] Z. Yin, J. Zhu, Q. He, X. Cao, C. Tan, H. Chen, Q. Yan, H. Zhang, *Adv. Energy Mater.* **2014**, *4*, 1300574.
[204] S. Wu, Q. He, C. Tan, Y. Wang, H. Zhang, *Small* **2013**, *9*, 1160.
[205] Q. He, S. Wu, Z. Yin, H. Zhang, *Chem. Sci.* **2012**, *3*, 1764.
[206] X. Qi, C. Tan, J. Wei, H. Zhang, *Nanoscale* **2013**, *5*, 1440.
[207] X. Qi, K. Y. Pu, H. Li, X. Zhou, S. Wu, Q. L. Fan, B. Liu, F. Boey, W. Huang, H. Zhang, *Angew. Chem. Int. Ed.* **2010**, *49*, 9426.
[208] X. Cao, Z. Zeng, W. Shi, P. Yep, Q. Yan, H. Zhang, *Small* **2013**, *9*, 1703.
[209] A. K. Geim, *Science* **2009**, *324*, 1530.
[210] C. Berger, Z. Song, X. Li, X. Wu, N. Brown, C. Naud, D. Mayou, T. Li, J. Hass, A. N. Marchenkov, E. H. Conrad, P. N. First, W. A. d. Heer, *Science* **2006**, *312*, 1191.
[211] T. Ohta, A. Bostwick, T. Seyller, K. Horn, E. Rotenberg, *Science* **2006**, *313*, 951.
[212] P. W. Sutter, J.-I. Flege, E. A. Sutter, *Nat. Mater.* **2008**, *7*, 406.
[213] G. Eda, G. Fanchini, M. Chhowalla, *Nat. Nanotechnol.* **2008**, *3*, 270.
[214] C. Gómez-Navarro, R. T. Weitz, A. M. Bittner, M. Scolari, A. Mews, M. Burghard, K. Kern, *Nano Lett.* **2007**, *7*, 3499.
[215] S. Gilje, S. Han, M. Wang, K. L. Wang, R. B. Kaner, *Nano Lett.* **2007**, *7*, 3394.
[216] C. Vallés, C. Drummond, H. Saadaoui, C. A. Furtado, M. He, O. Roubeau, L. Ortolani, M. Monthioux, A. Pénicaud, *J. Am. Chem. Soc.* **2008**, *130*, 15802.
[217] X. Li, G. Zhang, X. Bai, X. Sun, X. Wang, E. Wang, H. Dai, *Nat. Nanotechnol.* **2008**, *3*, 538.
[218] X. Li, W. Cai, J. An, S. Kim, J. Nah, D. Yang, R. Piner, A. Velamakanni, I. Jung, E. Tutuc, S. K. Banerjee, L. Colombo, R. S. Ruoff, *Science* **2009**, *324*, 1312.
[219] A. Reina, X. Jia, J. Ho, D. Nezich, H. Son, V. Bulovic, M. S. Dresselhaus, J. Kong, *Nano Lett.* **2008**, *9*, 30.
[220] X. Li, Y. Zhu, W. Cai, M. Borysiak, B. Han, D. Chen, R. D. Piner, L. Colombo, R. S. Ruoff, *Nano Lett.* **2009**, *9*, 4359.
[221] A. Reina, H. Son, L. Jiao, B. Fan, M. S. Dresselhaus, Z. Liu, J. Kong, *J. Phys. Chem. C* **2008**, *112*, 17741.
[222] L. Song, L. Ci, W. Gao, P. M. Ajayan, *ACS Nano* **2009**, *3*, 1353.
[223] J. D. Caldwell, T. J. Anderson, J. C. Culbertson, G. G. Jernigan, K. D. Hobart, F. J. Kub, M. J. Tadjer, J. L. Tedesco, J. K. Hite, M. A. Mastro, R. L. Myers-Ward, C. R. Eddy, P. M. Campbell, D. K. Gaskill, *ACS Nano* **2010**, *4*, 1108.
[224] S. Bae, H. Kim, Y. Lee, X. Xu, J.-S. Park, Y. Zheng, J. Balakrishnan, T. Lei, H. R. Kim, Y. I. Song, Y.-J. Kim, K. S. Kim, B. Özyilmaz, J.-H. Ahn, B. H. Hong, S. Iijima, *Nat. Nanotechnol.* **2010**, *5*, 574.
[225] R. Nair, P. Blake, A. Grigorenko, K. Novoselov, T. Booth, T. Stauber, N. Peres, A. Geim, *Science* **2008**, *320*, 1308.
[226] C. M. Weber, D. M. Eisele, J. P. Rabe, Y. Liang, X. Feng, L. Zhi, K. Müllen, J. L. Lyon, R. Williams, D. A. V. Bout, K. J. Stevenson, *Small* **2010**, *6*, 184.
[227] F. Güneş, G. H. Han, K. K. Kim, E. S. Kim, S. J. Chae, M. H. Park, H.-K. Jeong, S. C. Lim, Y. H. Lee, *Nano* **2009**, *4*, 83.
[228] J. K. Wassei, R. B. Kaner, *Mater. Today* **2010**, *13*, 52.
[229] T. Wehling, K. Novoselov, S. Morozov, E. Vdovin, M. Katsnelson, A. Geim, A. Lichtenstein, *Nano Lett.* **2008**, *8*, 173.
[230] P. Blake, P. D. Brimicombe, R. R. Nair, T. J. Booth, D. Jiang, F. Schedin, L. A. Ponomarenko, S. V. Morozov, H. F. Gleeson, E. W. Hill, A. K. Geim, K. S. Novoselov, *Nano Lett.* **2008**, *8*, 1704.

[231] F. Schedin, A. Geim, S. Morozov, E. Hill, P. Blake, M. Katsnelson, K. Novoselov, *Nat. Mater.* **2007**, *6*, 652.
[232] K. K. Kim, A. Reina, Y. Shi, H. Park, L.-J. Li, Y. H. Lee, J. Kong, *Nanotechnology* **2010**, *21*, 285205.
[233] V. C. Tung, L.-M. Chen, M. J. Allen, J. K. Wassei, K. Nelson, R. B. Kaner, Y. Yang, *Nano Lett.* **2009**, *9*, 1949.
[234] C. Jeong, P. Nair, M. Khan, M. Lundstrom, M. A. Alam, *Nano Lett.* **2011**, *11*, 5020.
[235] I. N. Kholmanov, C. W. Magnuson, A. E. Aliev, H. Li, B. Zhang, J. W. Suk, L. L. Zhang, E. Peng, S. H. Mousavi, A. B. Khanikaev, R. Piner, G. Shvets, R. S. Ruoff, *Nano Lett.* **2012**, *12*, 5679.
[236] J. Chen, H. Bi, S. Sun, Y. Tang, W. Zhao, T. Lin, D. Wan, F. Huang, X. Zhou, X. Xie, M. Jiang, *ACS Appl. Mater. Interfaces* **2013**, *5*, 1408.
[237] H. Jiang, K.-s. Moon, Y. Li, C. Wong, *Chem. Mater.* **2006**, *18*, 2969.
[238] R. Zhang, K.-s. Moon, W. Lin, C. Wong, *J. Mater. Chem.* **2010**, *20*, 2018.
[239] S. Jeong, K. Woo, D. Kim, S. Lim, J. S. Kim, H. Shin, Y. Xia, J. Moon, *Adv. Funct. Mater.* **2008**, *18*, 679.
[240] S. Jeong, H. C. Song, W. W. Lee, S. S. Lee, Y. Choi, W. Son, E. D. Kim, C. H. Paik, S. H. Oh, B.-H. Ryu, *Langmuir* **2011**, *27*, 3144.
[241] D. Huang, F. Liao, S. Molesa, D. Redinger, V. Subramanian, *J. Electrochem. Soc.* **2003**, *150*, G412.
[242] S. Yao, Y. Zhu, *Nanoscale* **2014**, *6*, 2345.
[243] D. J. Cohen, D. Mitra, K. Peterson, M. M. Maharbiz, *Nano Lett.* **2012**, *12*, 1821.
[244] Z. Cui, F. R. Poblete, G. Cheng, S. Yao, X. Jiang, Y. Zhu, *J. Mater. Res.* **2014**, DOI: 10.1557/jmr.2014.347.
[245] S.-J. Woo, J.-H. Kong, D.-G. Kim, J.-M. Kim, *J. Mater. Chem. C* **2014**, *2*, 4415.
[246] D. Wang, H. Li, M. Li, H. Jiang, M. Xia, Z. Zhou, *J. Mater. Chem. C* **2013**, *1*, 2744.
[247] S. C. Mannsfeld, B. C. Tee, R. M. Stoltenberg, C. V. H. Chen, S. Barman, B. V. Muir, A. N. Sokolov, C. Reese, Z. Bao, *Nat. Mater.* **2010**, *9*, 859.
[248] Y. Bar-Cohen, in *Proceedings of SPIE Smart Structures and Materials*, Vol. *4695* (Ed: Y. Bar-Cohen), SPIE, San Diego, CA, USA.
[249] Z. Yu, W. Yuan, P. Brochu, B. Chen, Z. Liu, Q. Pei, *Appl. Phys. Lett.* **2009**, *95*, 192904.
[250] T. Mirfakhrai, J. D. Madden, R. H. Baughman, *Mater. Today* **2007**, *10*, 30.
[251] X. Zhao, Q. Wang, *Appl. Phys. Rev.* **2014**, *1*, 021304.
[252] S. Shian, R. M. Diebold, A. McNamara, D. R. Clarke, *Appl. Phys. Lett.* **2012**, *101*, 061101.
[253] W. Yuan, L. Hu, Z. Yu, T. Lam, J. Biggs, S. M. Ha, D. Xi, B. Chen, M. K. Senesky, G. Grüner, Q. Pei, *Adv. Mater.* **2008**, *20*, 621.
[254] S. Rosset, H. R. Shea, *Appl. Phys. A* **2013**, *110*, 281.
[255] K. Xie, B. Wei, *Adv. Mater.* **2014**, *26*, 3592.
[256] C. Yan, P. S. Lee, *Small* **2014**, *10*, 3443.
[257] T. Chen, L. Dai, *Mater. Today* **2013**, *16*, 272.
[258] L. L. Zhang, X. Zhao, *Chem. Soc. Rev.* **2009**, *38*, 2520.
[259] Y. Zhu, S. Murali, M. D. Stoller, K. Ganesh, W. Cai, P. J. Ferreira, A. Pirkle, R. M. Wallace, K. A. Cychosz, M. Thommes, D. Su, E. A. Stach, R. S. Ruoff, *Science* **2011**, *332*, 1537.
[260] X. Cao, Z. Yin, H. Zhang, *Energy Environ. Sci.* **2014**, *7*, 1850.
[261] X. Li, T. Gu, B. Wei, *Nano Lett.* **2012**, *12*, 6366.
[262] M. Yu, Y. Zhang, Y. Zeng, M. S. Balogun, K. Mai, Z. Zhang, X. Lu, Y. Tong, *Adv. Mater.* **2014**, *26*, 4724.
[263] J. Zang, C. Cao, Y. Feng, J. Liu, X. Zhao, *Sci. Rep.* **2014**, *4*, 6492.
[264] Y. Zhou, Y. Bayram, F. Du, L. Dai, J. L. Volakis, *IEEE Trans. Antennas Propag.* **2010**, *58*, 2169.
[265] L. Song, A. C. Myers, J. Adams, Y. Zhu, *ACS Appl. Mater. Interfaces* **2014**, *6*, 4248.
[266] T. Rai, P. Dantes, B. Bahreyni, W. S. Kim, *IEEE Electron Device Lett.* **2013**, *34*, 544.
[267] C. Yan, J. Wang, X. Wang, W. Kang, M. Cui, C. Y. Foo, P. S. Lee, *Adv. Mater.* **2014**, *26*, 943.
[268] C. Yan, W. Kang, J. Wang, M. Cui, X. Wang, C. Y. Foo, K. J. Chee, P. S. Lee, *ACS Nano* **2013**, *8*, 316.
[269] G. D. Moon, G. H. Lim, J. H. Song, M. Shin, T. Yu, B. Lim, U. Jeong, *Adv. Mater.* **2013**, *25*, 2707.
[270] G. Ruffini, S. Dunne, E. Farrés, J. Marco-Pallarés, C. Ray, E. Mendoza, R. Silva, C. Grau, *Sens. Actuators, A* **2006**, *132*, 34.
[271] G. Ruffini, S. Dunne, L. Fuentemilla, C. Grau, E. Farres, J. Marco-Pallares, P. Watts, S. Silva, *Sens. Actuators, A* **2008**, *144*, 275.
[272] H.-C. Jung, J.-H. Moon, D.-H. Baek, J.-H. Lee, Y.-Y. Choi, J.-S. Hong, S.-H. Lee, *IEEE Trans. Biomed. Eng.* **2012**, *59*, 1472.
[273] A. Gruetzmann, S. Hansen, J. Müller, *Physiol. Meas.* **2007**, *28*, 1375.
[274] J.-Y. Baek, J.-H. An, J.-M. Choi, K.-S. Park, S.-H. Lee, *Sens. Actuators, A* **2008**, *143*, 423.
[275] A. C. Myers, H. Huang, Y. Zhu, *RSC Adv.* DOI: 10.1039/C4RA15101A.
[276] Z. Fan, J. C. Ho, T. Takahashi, R. Yerushalmi, K. Takei, A. C. Ford, Y. L. Chueh, A. Javey, *Adv. Mater.* **2009**, *21*, 3730.
[277] L.-L. Wang, B.-K. Tay, K.-Y. See, Z. Sun, L.-K. Tan, D. Lua, *Carbon* **2009**, *47*, 1905.
[278] F. C. Krebs, M. Jørgensen, K. Norrman, O. Hagemann, J. Alstrup, T. D. Nielsen, J. Fyenbo, K. Larsen, J. Kristensen, *Sol. Energy Mater. Sol. Cells* **2009**, *93*, 422.
[279] V. H. Pham, T. V. Cuong, S. H. Hur, E. W. Shin, J. S. Kim, J. S. Chung, E. J. Kim, *Carbon* **2010**, *48*, 1945.
[280] H.-H. Lee, K.-S. Chou, K.-C. Huang, *Nanotechnology* **2005**, *16*, 2436.
[281] J. Perelaer, B. J. de Gans, U. S. Schubert, *Adv. Mater.* **2006**, *18*, 2101.
[282] K. Kordás, T. Mustonen, G. Tóth, H. Jantunen, M. Lajunen, C. Soldano, S. Talapatra, S. Kar, R. Vajtai, P. M. Ajayan, *Small* **2006**, *2*, 1021.
[283] W. R. Small, *Small* **2007**, *3*, 1500.
[284] P. Chen, H. Chen, J. Qiu, C. Zhou, *Nano Res.* **2010**, *3*, 594.
[285] A. Mahajan, L. F. Francis, C. D. Frisbie, *ACS Appl. Mater. Interfaces* **2013**, *6*, 1306.
[286] C. S. Jones, X. Lu, M. Renn, M. Stroder, W.-S. Shih, *Microelectron. Eng.* **2010**, *87*, 434.
[287] D. Zhao, T. Liu, J. G. Park, M. Zhang, J.-M. Chen, B. Wang, *Microelectron. Eng.* **2012**, *96*, 71.
[288] J. Seo, H. Lee, S. Lee, T. I. Lee, J. M. Myoung, T. Lee, *Small* **2012**, *8*, 1614.
[289] H. Zhu, B. B. Narakathu, Z. Fang, A. T. Aijazi, M. Joyce, M. Atashbar, L. Hu, *Nanoscale* **2014**, *6*, 9110.
[290] S. P. Lacour, J. Jones, S. Wagner, T. Li, Z. Suo, *Proc. IEEE* **2005**, *93*, 1459.
[291] F. Xu, J. W. Durham III, B. J. Wiley, Y. Zhu, *ACS Nano* **2011**, *5*, 1556.
[292] T. Jiang, R. Huang, Y. Zhu, *Adv. Funct. Mater.* **2014**, *24*, 396.